

AD-786 528

**EVALUATION OF BACK-BLAST PRESSURES
PRODUCED BY A WING-MOUNTED 105-MM
RECOILLESS RIFLE**

William N. Lee, et al

Kaman AviDyne

Prepared for:

Watervliet Arsenal

July 1974

DISTRIBUTED BY:

NTIS

**National Technical Information Service
U. S. DEPARTMENT OF COMMERCE
5285 Port Royal Road, Springfield Va. 22151**

ACCESSION for	
NTIS	White Section <input checked="" type="checkbox"/>
DIC	Dist. Section <input type="checkbox"/>
UNCLASSIFIED	<input type="checkbox"/>
JUSTIFICATION	
BY	
DISTRIBUTION/AVAILABILITY CODES	
Dist.	AVAIL. and/or SPECIAL
A	

DISPOSITION

Destroy this report when it is no longer needed. Do not return it to the originator.

DISCLAIMER

The findings in this report are not to be construed as an official Department of the Army position unless so designated by other authorized documents.

ic

UNCLASSIFIED

SECURITY CLASSIFICATION OF THIS PAGE (When Data Entered)

REPORT DOCUMENTATION PAGE		READ INSTRUCTIONS BEFORE COMPLETING FORM
1. REPORT NUMBER WVT-CR-74023	2. JOVT ACCESSION NO.	3. RECIPIENT'S CATALOG NUMBER AD-786 528
4. TITLE (and Subtitle) EVALUATION OF BACK-BLAST PRESSURES PRODUCED BY A WING-MOUNTED 105-MM RECOILLESS RIFLE		5. TYPE OF REPORT & PERIOD COVERED Final Oct. 72 - July 73
7. AUTHOR(s) William N. Lee J. Ray Ruetenik Robert Smiley Norman P. Hobbs		6. PERFORMING ORG. REPORT NUMBER Kaman Avidyne TR-97
9. PERFORMING ORGANIZATION NAME AND ADDRESS Kaman Avidyne Burlington, Mass.		8. CONTRACT OR GRANT NUMBER(s) DAAF07-73-C-0163
11. CONTROLLING OFFICE NAME AND ADDRESS Development Engineering Directorate RDD-SE Watervliet Arsenal, Watervliet, N.Y.		10. PROGRAM ELEMENT, PROJECT, TASK AREA & WORK UNIT NUMBERS AMCMS: 513F.12.05014.02 DA Proj. No. 1F163206D050
14. MONITORING AGENCY NAME & ADDRESS (if different from Controlling Office)		12. REPORT DATE July 1974
		13. NUMBER OF PAGES 71
		15. SECURITY CLASS. (of this report) UNCLASSIFIED
		15a. DECLASSIFICATION/DOWNGRADING SCHEDULE
16. DISTRIBUTION STATEMENT (of this Report) Approved for public release; distribution unlimited.		
17. DISTRIBUTION STATEMENT (of the abstract entered in Block 20, if different from Report)		
18. SUPPLEMENTARY NOTES		
19. KEY WORDS (Continue on reverse side if necessary and identify by block number)		
AH-1G Blast Computer Codes Helicopter	Nozzles Pressure Distribution Recoilless Rifle	Reproduced by NATIONAL TECHNICAL INFORMATION SERVICE U S Department of Commerce Springfield VA 22151
20. ABSTRACT (Continue on reverse side if necessary and identify by block number)		
<p>Results are presented from an analytical study to develop means of reducing the back-blast pressures produced on the tail boom of an AH-1G helicopter by the firing of a 105-mm wing-mounted recoilless rifle.</p> <p>Computer codes were developed for predicting the back-blast fields and are partially substantiated by comparisons of calculated pressures with results from recent Picatinny firing tests. The desirability of reducing back-blast pressures through use of a multiple nozzle and by varying the (SEE REVERSE SIDE)</p>		

UNCLASSIFIED

SECURITY CLASSIFICATION OF THIS PAGE(When Data Entered)

Block No. 20 ABSTRACT (Continued)

firing chamber pressure profile is explored. It is found that the blast-field pressures can be reduced significantly by decreasing the average chamber pressure during the first 4 milliseconds after diaphragm burst.

ia

UNCLASSIFIED

SECURITY CLASSIFICATION OF THIS PAGE(When Data Entered)

TR-97

**KAMAN AVIDYNE
A DIVISION OF KAMAN SCIENCES CORPORATION
BURLINGTON, MASSACHUSETTS**

**EVALUATION OF BACK-BLAST PRESSURES
PRODUCED BY A WING-MOUNTED
105-MM RECOILLESS RIFLE**

By

**William N. Lee
Robert Smiley
J. Ray Ruetenik
Norman P. Hobbs**

July 30, 1973

For

**WATERVLIET ARSENAL
WATERVLIET, NEW YORK**

ib

FOREWORD

This report was prepared by the Kaman AvIDyne Division of Kaman Sciences Corporation, Burlington, Massachusetts, for Watervliet Arsenal under Contract DAAF07-73-C-0163. Mr. Charles Andrade was the project monitor for Watervliet Arsenal. Dr. J. Ray Ruetenik served as project leader for Kaman AvIDyne.

Appreciation is expressed to Mr. Donald Spring, Mr. Andrade and Major John Adams of the Watervliet Arsenal for their critical comments on the work at a number of meetings through the contract period.

ABSTRACT

Results are presented from an analytical study to develop means of reducing the back-blast pressures produced on the tail boom of an AH-1G helicopter by the firing of a 105-mm wing-mounted recoilless rifle.

Computer codes were developed for predicting the back-blast fields and are partially substantiated by comparisons of calculated pressures with results from recent Picatinny firing tests. The desirability of reducing back-blast pressures through use of a multiple nozzle and by varying the firing chamber pressure profile is explored. It is found that the blast-field pressures can be reduced significantly by decreasing the average chamber pressure during the first 4 milliseconds after diaphragm burst.

TABLE OF CONTENTS

	<u>Page</u>
FOREWORD	ii
ABSTRACT	iii
1. INTRODUCTION	1
2. THE AH-1G HELICOPTER	3
3. BLAST-FIELD CALCULATIONS	4
3.1 Analytical Approach	4
3.2 Internal Flow Code (S1D).	5
3.3 External Flow Code (S2D).	6
4. CORRELATION OF CALCULATED AND EXPERIMENTAL BLAST FIELDS	7
5. EVALUATION OF MULTIPLE NOZZLE CONCEPT	10
6. PARAMETRIC CHAMBER PRESSURE STUDIES	12
6.1 Chamber Pressure Profiles	13
6.2 Variation of Peak Reflected Overpressure with Peak Chamber Pressure	14
6.3 Effect of Rate of Chamber Pressure Rise	16
6.4 Effect of Chamber Pressure Decay Shape	19
6.5 Variation of Muzzle Velocity with Peak Chamber Pressure	19
6.6 Variation of Peak Reflected Overpressure with Muzzle Velocity	20
6.7 Summary of Principal Results	22

TABLE OF CONTENTS (CONT.)

	<u>Page</u>
7. CONCLUSIONS	23
8. RECOMMENDATIONS	25
REFERENCES	27
APPENDIX A	
S1D CODE	50
APPENDIX B	
S2D CODE	52
APPENDIX C	
THERMODYNAMIC CONSIDERATIONS	57

LIST OF FIGURES

<u>Figure</u>		<u>Page</u>
1	AH-1G Helicopter Geometry	31
2	Overall Blast Field Problem	32
3	Comparison of Computed Nozzle Exit Pressures for Transient and Quasi-Steady Flow	33
4	Nozzle and External Flow Representation	34
5	Chamber Pressure Profiles of Picatinny Tests	35
6	Experimental and Calculated Free-Field Overpressure Time Histories at Two Stations 48" from the Gun Axis.	36
7	Gun Length Needed with a Multiple Nozzle to Reduce Reflected Overpressure to 5 psi at 60 inches from Gun Axis	37
8	Chamber Pressure Profiles for Peak Pressure Studies for Constant Muzzle Velocity.	38
9	Chamber Pressure Profile Family 2 for Peak Pressure Studies with a Single Profile Shape	39
10	Chamber Pressure Profiles for Rise Rate Studies	40
11	Chamber Pressure Profiles for Initial Buildup Studies	41
12	Chamber Pressure Profiles for Decay Shape Studies	42
13	Two Chamber Pressure Profiles for Short Times to Peak Pressure	43
14	Effect of Peak Chamber Pressure on Peak Reflected Pressure.	44
15	Comparison of Chamber Pressure Profiles 3 and 6	45
16	Effect of Chamber Pressure Rise Rate on Reflected Pressure.	46
17	Variation of Peak Reflected Pressure with Chamber Pressure at 4 msec	47

LIST OF FIGURES (CONCL.)

<u>Figure</u>		<u>Page</u>
18	Variation of Peak Reflected Pressure with Average Chamber Pressure from 0-4 msec	48
19	Variation of Peak Reflected Pressure with Muzzle Velocity for a 25-Pound Projectile	49
A.1	Sample Pressure Profile Inside a Nozzle	51
B.1	Cell Layout Employed in S2D Code for Computing the Back-Blast Pressure Field	54
B.2	Sample Printout for S2D Code	55
B.3	Three-Dimensional Plot of External Peak Overpressure Field	56

LIST OF TABLES

<u>Table</u>		<u>Page</u>
1	Positions on the AH-1G Tail Boom	28
2	Comparison of Experimental and Calculated Field Overpressures	29
3	Conditions and Results of Parametric Studies	30

LIST OF COMMON SYMBOLS

p	overpressure (psig)
\bar{p}_r	peak reflected overpressure (psig)
p_{ch}	instantaneous chamber pressure (psia)
p_{cha}	average chamber pressure from 0 - 4 msec after diaphragm burst (psia)
p_{ch4}	chamber pressure 4 msec after diaphragm burst (psia)
\bar{p}_{ch}	peak chamber pressure (psia)
t	time (msec)
T	time to peak chamber pressure (msec)
v	muzzle velocity

1. INTRODUCTION

As a result of recent U.S. Army interest in the development of recoilless guns to be mounted on airborne vehicles, a number of experimental and analytical studies have been performed to assess the back-blast pressures produced by such guns and to assess their damage potential for the launching vehicle. It has been found from such studies that the back-blast fields of such guns can present severe hazards to the launching vehicle, which, in turn, can severely limit the muzzle velocities which can be safely obtained with a given projectile, either with or without supplementary rocket-assisted propulsion. However, as yet, no satisfactory analytical or empirical techniques have been developed to provide accurate estimates of back-blast pressures and damage for untested configurations.

As part of this general development of recoilless airborne guns, the U.S. Army has been developing a 105-mm rifle to be used on the AH-1G (Cobra) Helicopter. As an aid to this development effort, Kaman AviDyne has developed several computer codes for predicting the back-blast pressure fields of recoilless rifles, applied these codes to predict back-blast fields for a wide variety of firing conditions, and evaluated various measures for reducing the back-blast pressures. Results of these studies are presented in this report, arranged as follows.

Section 2 indicates the basic helicopter-gun system under consideration. Section 3, supplemented by Appendices A-C, describes the flow idealizations and computational procedures developed and used for computing back-blast fields.

Section 4 presents a partial evaluation of the realism of the developed computer codes through comparisons of calculated back-blast pressures with recent Picatinny test results.

Sections 5 and 6 deal with theoretical calculations of back-blast pressures for a variety of nozzle configurations and firing chamber profiles. As a basic ground rule for these studies, it is assumed the AH-1G can withstand reflected back-blast overpressures of 5 psi, and methods are sought to reduce back-blast pressures to this level.

Section 5 presents an evaluation of the feasibility of reducing back-blast pressures by replacing the standard gun nozzle by a multiple nozzle.

Section 6 presents and discusses calculated back-blast pressure fields for a wide variety of gun firing chamber pressure profiles and indicates various means for reducing the back-blast fields by varying the profile.

Sections 7 and 8 present the major conclusions and recommendations obtained.

2. THE AH-1G HELICOPTER

The present study was primarily centered on the evaluation of back-blast pressures on the tail boom of an AH-1G helicopter due to the action of a recoilless rifle mounted on the wing, 60 inches from the tail-boom centerline. The basic helicopter and gun geometry involved are shown in Figure 1. Also indicated in Figure 1 and in Table 1 are the locations of several positions on the helicopter (A, B, C) for which pressure field calculation results are presented in later parts of this report.

The first position (A), hereafter called the critical position, is about 96 inches behind the nozzle exit in the helicopter panel section running from boom stations (B.S.) 59.50 to 80.44. According to calculations by Southwest Research Institute for Watervliet Arsenal for the AH-1G helicopter (Ref. 1) and experimental results from the "Dial Pack" high explosive test for the UH-1B helicopter (Ref. 2), this position appears to be in a critical area for structural failure from a 105-mm recoilless rifle back blast.

The second position (B) corresponds to a rear tail-boom section arbitrarily taken as 240 inches behind the nozzle exit (B.S. 214). The third position (C) is near the rear tip of the vertical tail.

3. BLAST-FIELD CALCULATIONS

This section describes briefly the assumptions and procedures used in this study for computing the blast pressure field produced by the back blast from a recoilless rifle.

3.1 Analytical Approach

The overall back-blast problem was idealized as shown in Figure 2. The gun chamber is considered to be a chamber having prescribed pressure and density time histories, and which is connected through a diaphragm to a convergent-divergent critical flow nozzle exiting into an initially undisturbed atmosphere. The diaphragm is assumed to break at some prescribed pressure (several hundred psi), after which the chamber gas is assumed to flow adiabatically through the nozzle according to the transient one-dimensional flow relationships for a perfect gas of constant specific-heat ratio. The entire flow field is considered to be axially symmetrical.

A gun barrel with a projectile inside is connected to the front end of the chamber. The theoretical exit velocity of the projectile is estimated by neglecting projectile air drag and friction and the pressure drop from the chamber to the projectile. Since muzzle velocity is only computed to indicate trends of chamber-pressure histories, these idealizations are considered acceptable.

For convenience, the back-blast flow problem was broken down into two computer codes, one to compute the internal nozzle flow, designated S1D, and

another to compute the external field flow, designated S2D. Brief descriptions of these codes are given in Appendices A and B and related assumptions on needed gas thermodynamic relationships are discussed in Appendix C.

3.2 Nozzle Flow Code (S1D)

The S1D code computes the time histories of pressure, density and fluid velocities at the exit of the nozzle for given chamber pressure and density time histories and was originally developed for use in determining initial conditions for the S2D external flow code. However, it was found that exit conditions calculated from the S1D code (for transient nozzle flow) differed so little from predictions made on the basis of simple quasi-steady one-dimensional flow equations that there was no need or justification for extensive use of the S1D code in the present study.

This point is illustrated in Figure 3, which presents time histories of nozzle exit pressure according to the S1D code and to the steady-state flow equations (note the discontinuity in the time scale). The exit pressures for the two calculations are seen to be very similar except for the first quarter of a millisecond. During the latter time, the S1D code predicts the passage of a high intensity but short duration shock wave out of the nozzle exit^{*}. However, the duration of this shock wave is only 0.1 millisecond, which proved, according to S2D calculations, to be too short a time to have any significant effect on the peak external field pressures in regions of interest for the

* It might be noted that recent Picatinny measurements of nozzle internal pressure during Test Round 48 (Ref. 3) indicated no definite large shock of this type passing through the nozzle.

helicopter problem. For example, for the critical position A on the helicopter (see Section 2), the peak field pressure was only 10% higher with the nozzle exit conditions predicted by the S1D code than by the quasi-steady method, and there was no significant difference for the other two positions considered (B and C).

In view of the above considerations, use of the S1D code was discontinued and all calculated results presented hereafter in this report are based on quasi-steady nozzle flow relationships for the internal flow stage of the back-blast problem. By the term quasi-steady is meant that the flow at the nozzle exit corresponds to the steady-state flow that would exist for the same instantaneous conditions in the chamber.

3.3 External Flow Code (S2D)

The S2D code treats the problem shown in Figure 4, where a gas of known time-varying pressure, density and fluid velocity flows from a set of coaxial annular nozzles into an ambient field of known initial pressure and density. The figure illustrates the nozzle configuration for a 3-stage nozzle. The flow is assumed to be axially symmetrical and governed by the perfect-gas law with a constant specific-heat ratio.

In the computer simulations, the geometric flow field is composed of a set of coaxial annular cylindrical cells, having arbitrary radial thickness (Δr) and the same axial length (Δx), as indicated in Figure 4. For most of the studies the axial cell length was taken as about 7 inches and the radial cell thickness as about 3 inches.

Further discussion of the S2D code, including sample printouts, is given in Appendix B.

4. CORRELATION OF CALCULATED AND EXPERIMENTAL BLAST FIELDS

This section presents an evaluation of the degree of realism of the Kaman AviDyne S2D computer code described above for computing back-blast fields by means of comparisons of calculated field pressures with experimental data recently obtained by Picatinny Arsenal from firing tests of a recoilless rifle (Refs. 3 and 4). These firings were conducted using the Army 105-mm recoilless rifle standard nozzle (45°/15°, 4:1 area ratio, 3.43 inch dia. throat), hereafter called the standard nozzle.

Some experimental results of these tests are given in Figure 5 and Table 2, where Figure 5 presents chamber pressure profiles and Table 2 presents values of experimental peak free-field and reflected overpressures* for various locations in the blast field (x and r in Figure 1). The latter data were obtained with pressure transducers imbedded in a ground reflection plane located below and parallel to the gun axis. Also presented in Table 2 are calculated values of peak free-field and reflected overpressures, using the S2D code, where the calculated reflected overpressures were obtained by multiplying the calculated free-field overpressures by the theoretical reflected overpressure ratio for a normal shock**.

* All field pressures discussed in this report are expressed as overpressures (above ambient pressure).

** All calculated peak reflected pressures presented in this report were calculated in this manner.

The calculated peak overpressures in Table 2 vary from about 25% to 150% of the experimental values, being usually below the experimental values at the higher overpressure levels. For the test with the most extensive instrumentation and most consistent appearing experimental results (Round 13), agreement is considerably better, with the calculated values (in parentheses) varying from about 65% to 130% of the corresponding experimental values.

It may be noted that there appears to be a tendency for the experimental overpressures to significantly exceed the calculated values, particularly for large downstream distances. This is partly to be expected since most of the calculated values represent average values over distances of about 7 inches (typical axial cell length) or, equivalently, averages over times of about 0.5 millisecond, whereas some of the experimental values represent peak values of appreciably shorter duration.

A comparison of experimental and calculated time histories of free field overpressures is shown in Figure 6 for the conditions of Picatinny Arsenal Test Rounds 13 and 48 (Ref. 3). It may be noted that the calculated time histories follow the main trends of the experimental data fairly well and appear to represent an average of the experimental data over about several milliseconds. The calculated time histories for the greater distance from the nozzle ($x = 179''$) are seen to be displaced in time from the corresponding experimental time histories. However, this time difference does not necessarily have much significance since it is of the same order of magnitude as the uncertainty in the time at which the nozzle diaphragm bursts (which time had to be relatively arbitrarily selected for the calculations).

With respect to details, there are obvious differences between the calculated and experimental time histories in Figure 6, particularly for the field location closest to the nozzle (for $x = 83''$ in Figure 6). The experimental curves (for $x = 83''$) are seen to contain more frequent and larger peaks and some high frequency spikes and oscillations. One reason for the lesser detail structure in the predicted curves arises from the finite grid size, which, for the grid used, gives calculated pressure averages over a time period of about 0.5 millisecond rather than instantaneous pressures. However, it appears more likely that these experimental irregularities and larger peaks result from deviations of the chamber-pressure time history from the assumed smooth profiles of Figure 5 (e.g., some profiles actually have large short-duration pressure spikes in the early pressure buildup stages). Also there is considerable experimental evidence and some calculated confirmation that some of the gun propellant is ejected unburned from the nozzle and burns in the external field, which effect (not included in the present S2D code) could lead to both higher and more irregular external field pressures than those calculated without considering this effect.

The major results of the above comparison tend to confirm the predictions of the KA S2D code, and indicate that this code offers a fairly realistic tool for investigating effects of gun configuration and propellant factors on the blast fields. From the four runs compared, no conclusive trends of difference between the experimental data and the code predictions are evident, so the predictions of the Kaman S2D code are used hereafter directly as computed.

5. EVALUATION OF MULTIPLE-NOZZLE CONCEPT

A significant part of the present study was devoted to consideration of the possibilities of reducing back-blast pressures by replacing the currently used single nozzle by a set of multiple coaxial nozzles (e.g., see Fig. 4). The basic ground rule for this study was to determine whether such a nozzle could be constructed which could reduce the reflected pressures on the AH-1G to 5 psi without requiring an increase in the total gun length from its present length of 157 inches to more than 170 inches.

The following assumptions and calculations were made to explore this concept. Each nozzle segment was taken to expand the flow to Mach 2.65 at the exit, as it turned out that higher Mach numbers gave higher pressures in the field. The percentage of flow in each nozzle segment was varied in separate computer runs for each multiple nozzle in order to minimize the peak overpressure along a line 60 inches laterally from the nozzle axis extending from the nozzle to an axial distance 26 feet downstream from the standard nozzle exit, the most rearward point of an AH-1G. The chamber pressure profile used for all S2D code calculations for multiple nozzles was chosen for convenience as a step pressure rise to 7722 psi. The corresponding calculated total gun length required to reduce the peak reflected overpressure to 5 psi (compared to the standard gun length of 157 inches) for this hypothetical step-pressure chamber profile is given in Figure 7.

Estimates of the corresponding gun length requirements for a realistic chamber profile, with a time-varying pressure selected as the profile for

Picatinny test Round 13 (with a peak pressure of 7750 psi and a calculated muzzle velocity of about 780 fps for a 25 pound projectile), are also presented in Figure 7. These gun lengths were scaled from the step-pressure results by using the 30-percent decrease in nozzle extension obtained for a single nozzle with the variable pressure profile, according to S2D calculations.

The resulting total gun length estimates given in Figure 7 indicate that the minimum gun length that could be achieved with a multiple nozzle of 6 segments for the variable pressure profile is about 255 inches. Further increases in the number of nozzle segments would not be expected to reduce the overall gun length by more than an inch.

The above observations indicate that the desired field pressure reductions to 5 psi cannot be obtained with a 170-inch multiple nozzle alone. However, when used in conjunction with other pressure reduction measures discussed below, the demonstrated pressure reduction capabilities of multiple nozzles may still prove of practical value.

6. PARAMETRIC CHAMBER PRESSURE STUDIES

In order to evaluate the effect upon back-blast pressures of varying the chamber pressure history, calculations were made of field pressures for the standard nozzle with the KA S2D code for the chamber pressure profiles shown in Figures 8-13* (see also Table 3). Results of these calculations, which are summarized in this section, offer a guide for estimating and reducing helicopter back-blast pressures over a wide range of conditions.

Calculations were made for chamber profiles giving muzzle velocities between 850 fps and 1800 fps for a 25-pound projectile. The lower limit is the minimum muzzle velocity stated to be of interest in the present contract specification and is somewhat higher than the velocities measured for all recent relevant Picatinny Arsenal test rounds known to KA (Refs. 3-4).

Field pressures are presented here for the three positions in the back-blast field designated in Section 2 as A (critical position), B (rear position) and C (tip position) (see Fig. 1).

For convenience of presentation, this section is divided into separate discussions of the following topics:

1. Description of chamber pressure profiles considered
2. Variation of peak reflected overpressure with peak chamber pressure
3. Effect of chamber pressure rise rate

*The zero time reference point in all chamber pressure profiles represents the time of nozzle diaphragm burst, not the earlier time at which the chamber pressure begins to rise after explosive ignition.

4. Effect of chamber pressure decay shape
5. Variation of peak chamber pressure with muzzle velocity
6. Variation of peak reflected overpressure with muzzle velocity
7. Summary of principal results

6.1 Chamber Pressure Profiles

The chamber pressure profiles No. 1 to 4, shown in Figure 8, are the basic profiles selected for determining the effect of chamber pressure variables on peak reflected overpressure in the field. Profile No. 1 is similar to the measured profile of Picatinny Round No. 13 and would give an ideal muzzle velocity of about 850 fps for a 25-pound projectile. Profiles No. 2 to 4 are designed so as to maintain the same muzzle velocity while progressively reducing the peak chamber pressure. The initial pressure for the profiles is equal to 500 psi, corresponding to equal diaphragm bursting pressures.

Variations of Profiles 1 and 2, referred to hereafter as Profile Families 1 and 2, respectively, were obtained essentially by simply scaling all pressures by a constant value. The resulting profiles are indicated by primes or double primes, as for example Profiles 2' and 2'' shown in Figure 9. The chamber pressure for Profile 2, times the ratio of the peak chamber pressure for Profile 2'' of 12,800 psi to the peak value of Profile 2 of 5,750 psi. As a slight departure from this rule, the initial pressure is maintained equal, as before.

In order to evaluate effects of chamber pressure rise rate, a second set of chamber pressure profiles, based on Profile 1, was generated by linearly increasing the time scale for all chamber pressures up to the time of peak chamber pressure. The resulting modified profiles considered are shown as Profiles 5 and 6 in Figure 10.

A third set of modified profiles, also of interest to evaluate chamber pressure rise rate effects, is shown in Figure 11. These profiles were derived from Profile 4 by shifting the Profile 4 curves, for times greater than 2 msec, to the right by 4 msec (for Profile 4A) or 10 msec (for Profile 4B) and arbitrarily selecting a low-pressure low-rise-rate variation for the initial pressure buildup stage.

The fourth set of modified profiles was generated to examine the effect of the chamber pressure decay rate. The resulting modifications of Profile 2 are designated as Profiles 7 and 8 in Figure 12.

A final set of profiles, shown in Figure 13, was selected to examine profiles with short (less than 4 msec) times to peak chamber pressure. (All other profiles had times to peak pressure greater than 4 msec.) This set consists of the profile for Picatinny Round 1 and an arbitrary truncation of this profile to a peak chamber pressure value of about half that for Round 1.

6.2 Variation of Peak Reflected Overpressure with Peak Chamber Pressure

The variation of peak reflected overpressure, \bar{p}_r , at the critical position (A in Figure 1) is plotted in Figure 14 for Profile Families 1 - 6 as a function of the peak chamber pressure \bar{p}_{ch} .

It is evident from Figure 14 that, in general, the peak reflected overpressure is not a simple function of the peak chamber pressure alone, since there is as much as a 2:1 variation in peak reflected overpressure at the lowest peak chamber pressure considered. However, for the Profile Families 1 to 4 of Figure 8 (including Profile 1', 2' and 2'') the calculated peak reflected overpressures in Figure 14 can be approximately considered to depend only on peak chamber pressure according to the empirical equation

$$\bar{p}_r = 0.029 \bar{p}_{ch}^{0.6} \quad (\text{critical position}) \quad (1)$$

shown on the figure. (Similar 0.6-power laws were obtained for positions B and C.)

Further evidence that the peak reflected overpressure cannot, in general, be simply related to peak chamber pressure can be obtained by examination of the peak reflected overpressures for Profiles 3 and 6, which profiles are presented together in Figure 15. It is evident from this figure that if peak chamber pressure were the dominant factor influencing the peak reflected overpressure, then the peak reflected overpressures for Profile 6 would be expected to be significantly greater than for Profile 3. However, the calculated peak reflected overpressures for Profile 3 (with the much lower peak chamber pressure) are greater than for Profile 6, or in other words, for this profile pair, a significant decrease in peak chamber pressure (from Profile 6) results in an increase in peak reflected overpressure*.

With respect to the question of scaling peak reflected overpressure data for a given peak chamber pressure to apply to similar chamber pressure profiles with different peak chamber pressures, it was found from calculation results for Profile Families 1 and 2, presented in Figure 14 (compare square and diamond symbols with Equation (1) curve), that the peak reflected overpressures vary approximately as the 0.6-power of the peak chamber pressure or (restating Equation (1) in a more general form):

*The reason for the greater field pressure for Profile 3 is that the early-time chamber pressure rise rate is greater than for Profile 6 (see Section 6.3).

$$\bar{p}_r = \bar{p}_{r,o} (\bar{p}_{ch}/\bar{p}_{ch,o})^{0.6} \quad (2)$$

where the subscript o designates the chamber and reflected pressure values for any known condition. Equation (2), used with pressure values from Table 3 could be expected to give at least a rough estimate of peak reflected overpressure for chamber pressure profiles similar to those of Table 3, and particularly so for the near-conventional Profile Families 1 and 2.

6.3 Effect of Rate of Chamber Pressure Rise

In view of the above evidence that peak chamber pressure is not, in general, an adequate index of the peak reflected overpressure for arbitrary chamber profiles, consideration is given here to the effect of the rate of rise of the chamber pressure prior to reaching its peak value.

Figure 16 compares the calculated peak reflected overpressures for three chamber profiles (shown in Figure 10) having the same peak chamber pressure of 8500 psi but different rise rates. (The overpressure ratios in this figure are plotted for the critical field position A in Figure 1, but also apply fairly well for positions B and C.) The data in Figure 16 demonstrate that decreasing the chamber pressure rise rate (i.e., increasing time to peak chamber pressure) results in decreased peak reflected overpressures. More specifically, it is seen that a decrease of chamber pressure rise rate of about 60% (corresponding to an increase in time to peak chamber pressure of 4 milliseconds) yields a reduction of peak field pressure to about 79% of the initial value for a typical test profile shape (Profile 1). It should be also noted that this reduction of peak reflected overpressure is accompanied by an increase of predicted muzzle velocity from 850 fps to 1135 fps (Table 3).

Another comparison for chamber pressure profiles having similar shapes but different initial rise rates can be made by comparing peak reflected overpressure values from Table 3 for Profiles 4, 4A and 4B of Figure 11. These data indicate substantially lower peak reflected overpressures for the profiles with lower initial chamber pressure rise rates. More specifically, reducing the initial pressure level and rise rate from that of Profile 4 to 4A reduces the peak reflected overpressure for the critical position by 45 percent and going to Profile 4B reduces it by 50 percent. It might also be noted that for the last case (Profile 4B), which corresponds to a muzzle velocity of 900 fps, the peak reflected overpressures are well below 5 psi for all positions.

The above observations suggest that the rate of chamber pressure buildup strongly influences the peak reflected overpressure and may be much more influential than the peak chamber pressure. Furthermore, it appears probable from an analysis of our limited number of calculated peak reflected overpressures (in Table 3) that it is not the maximum rate of chamber pressure rise which is important, but rather some average or effective rise rate which occurs within 2-4 msec after diaphragm burst (which is the zero time reference in all our chamber pressure profiles). As two relatively arbitrary indicators of this effective rise rate we selected the values of chamber pressure at 4 msec, p_{ch4} , and the average chamber pressure over the first 4 msec (after diaphragm burst), p_{cha} . Calculated peak reflected overpressure data (from Table 3) for the critical position in Figure 1 for all of the profiles listed in Table 3* are plotted against these two parameters in Figures 17 and 18, respectively.

* The peak pressures for Profiles 2, 7 and 8 in Table 3 are identical and are represented by a single point in both Fig. 17 and Fig. 18.

Considering first the parameter based on the chamber pressure at 4 msec, the data in Figure 17 indicate that the peak reflected overpressures for times to peak chamber pressure, T, greater than 4 msec appear to depend only on the parameter p_{ch4} and can be approximately described by an empirical square-root relationship (shown in Figure 17) of the form

$$\bar{p}_r = 0.095 p_{ch4}^{0.5} \quad (\text{critical position}) \quad (3)$$

for the critical position, and by similar square root relationships for other positions.

For the two profiles with times to peak chamber pressure less than 4 msec, the calculated peak reflected overpressures are seen to be higher in Figure 17 than for times greater than 4 msec, hence the usefulness of the p_{ch4} index and the associated Equation (3) appears limited to profiles with times to peak chamber pressure greater than 4 msec.

Next, considering the average chamber pressure index p_{cha} , the calculated peak reflected overpressure data in Figure 18 appear to depend approximately only on p_{cha} for all profiles and can be approximately represented by the empirical equation .

$$\bar{p}_r = 0.068 p_{cha}^{0.6} \quad (\text{critical position}) \quad (4)$$

Hence, the parameter p_{cha} appears to be the most useful and basic indicator of peak reflected overpressure which we have considered.

6.4 Effect of Chamber Pressure Decay Shape

The effect of the shape of the decay portion of the chamber pressure profile on peak reflected overpressure was calculated for the three profile variations shown in Figure 12. The results, given in Table 3 (see Profiles 2, 7 and 8), indicate essentially the same peak reflected overpressures for these three profiles, indicating that the decay or late-time shape of the chamber pressure profile has little influence on the peak reflected overpressures.

6.5 Variation of Muzzle Velocity with Peak Chamber Pressure

To relate some of the preceding observations of peak reflected overpressure to muzzle velocity, the following equation for ideal muzzle velocity is used. Here the chamber pressure is related to muzzle exit velocity, v , by integration of the projectile equation of motion over the time the projectile remains in the gun barrel, approximately* as

$$v = (a/m) \int p_{ch} dt \quad (5)$$

where

a is barrel cross-sectional area

m is projectile mass

p_{ch} is instantaneous chamber pressure

For further purposes, it is useful to develop an approximate relation for muzzle velocity in terms of peak chamber pressure. For each considered family

* All values of muzzle velocities presented in this report are ideal values based on Equation (5). Actual muzzle velocities would, of course, be somewhat different due to muzzle friction and pressure changes from the combustion chamber to the barrel.

of similar chamber pressure profiles with different peak chamber pressures, the muzzle velocities calculated from Equation (5) turn out to be usually almost linearly proportional to peak chamber pressure (\bar{p}_{ch}) and can be expressed as

$$v = (v/\bar{p}_{ch})_o \bar{p}_{ch} \quad (6)$$

where $(v/\bar{p}_{ch})_o$ is the value of v/\bar{p}_{ch} for any member of the family, and could be estimated from the data in Table 3 for the profile families in this report. Use of Equation (6) provides an estimate of muzzle velocity as a function of peak chamber pressure, which is used in Section 6.6 to relate reflected pressure variations to muzzle velocity changes.

6.6 Variation of Peak Reflected Overpressure with Muzzle Velocity

The present study results indicate that the relationship between peak reflected overpressure and muzzle velocity depends in too complex a manner on the parameters of the chamber pressure profile to permit any simple statements here for predicting peak reflected overpressure in terms of chamber pressure parameters. However, the calculated data of Table 3, as partly analyzed in Sections 6.2 and 6.4, do permit formulation of the following approximate scaling relationships and some comments can be made on what minimum peak reflected overpressures can be expected for various muzzle velocities of interest.

From the results of the preceding studies of peak reflected overpressures, chamber pressure and muzzle velocity in Sections 6.2 and 6.5, it follows by combining the approximate Equations (2) and (6) that the scaling relationship between peak reflected overpressures and muzzle velocity for similar chamber pressure profiles is given approximately as

$$\bar{p}_r = \bar{p}_{ro} (v/v_o)^{0.6} \quad (7)$$

where the subscript zero designates the values of peak reflected overpressure and muzzle velocity for any member of the same profile family.

Equation (7) indicates that for similar chamber pressure profiles, the peak reflected overpressure varies as the 0.6-power of the muzzle velocity. This relationship is also demonstrated in Figure 19 which presents values of peak reflected overpressure and muzzle velocities for the Profile Families 1 to 4B and several 0.6-power-law curves.

With regard to the lowest peak reflected overpressures which can be obtained for various muzzle velocities, it was calculated that for a 900-fps muzzle velocity (one of the lowest muzzle velocities considered of interest for this study), the peak reflected pressure for the critical position (A) could be reduced to 1.9 psi (to 1.9 psi for Position B and 3.7 psi for Position C) by using Profile 4B (Fig. 11).

No studies were made of profiles giving very low reflected pressures for muzzle velocities higher than 900 fps, but it might be noted that even the not particularly favorably shaped Profile 6 (Fig. 10), with a predicted muzzle velocity of 1135 fps, has a peak reflected overpressure of only 4.5 psi for the critical position (A) and pressures of 9.8 for positions B and C.

For the more nearly conventional chamber pressure profiles of Profile Families 1 to 4 in Figure 8, estimates were made of the maximum muzzle velocities which could be obtained without exceeding 5 psi at the critical position. These values were obtained from the 0.6 power lines in Figure 19 and are 530 fps for Profile Family 1, 790 fps for Profile Family 2, 890 fps for Profile Family 3, and 1350 fps for Profile Family 4.

6.7 Summary of Principal Results

The above-described parametric studies indicate that substantial reductions in back-blast peak reflected overpressures may be realized by modifying recent test chamber profiles in such a manner that the average chamber pressure over the first four milliseconds after diaphragm burst is reduced.

Through possible (although not necessarily practical) applications of these modifications it has been calculated that the peak reflected overpressures could be reduced below 5 psi for all positions of interest (see results for Positions A, B and C for Profile 4B in Table 3).

7. CONCLUSIONS

The principal conclusions of the studies described herein of back-blast pressures produced on an AH-1G helicopter by a recoilless rifle blast are presented below:

1. Calculations of free-field pressures at the helicopter tail boom using the Kaman AviDyne S2D code for the flow external to the nozzle and either quasi-steady relationships or the KA SID one-dimensional transient flow code for determining nozzle exit flow conditions gave about the same free-field pressures, indicating that a quasi-steady representation of the internal flow is adequate for back-blast calculations.
2. Free-field and reflected overpressures calculated using the S2D code are in fair agreement with experimental overpressures measured during recent firing tests of a 105-mm recoilless rifle at Picatinny Arsenal.
3. Back-blast pressures for a multiple-nozzle system, calculated by the S2D code, have shown that such a nozzle could produce appreciably reduced pressures on the tail section of an AH-1G helicopter. However, the length of nozzle required to reduce the reflected overpressures on the tail to 5 psi, by use of a multiple nozzle alone, appears to be too long to be considered practical at present.
4. Calculated back-blast field pressures for a variety of chamber pressure profiles indicate that reductions of peak reflected overpressures can be obtained without sacrificing muzzle velocity by modifying chamber pressure time histories to reduce the average chamber pressure during the first four milliseconds after diaphragm burst.

5. For the considered chamber pressure profile which gave the lowest field pressures (Profile 4B in Fig. 11), with a muzzle velocity of 900 fps for a 25-pound projectile, calculations indicate that the peak reflected blast overpressures on an AH-1G helicopter fuselage could be reduced below 5 psi.

8. RECOMMENDATIONS

The considerations of this report indicate that it should be possible to obtain muzzle velocities of at least 850 fps for a 25-pound projectile from a 105-mm recoilless rifle without producing back-blast damage to an AH-1G helicopter, based on the criterion of a 5-psi peak reflected overpressure. Such desired muzzle velocities could be obtained either by modifying the chamber pressure profile (as indicated herein), by adding a multiple nozzle, by hardening the present structure, or by some judicious combination of these measures. The following program is recommended to develop these possibilities.

The practicality of obtaining more favorable chamber pressures as indicated herein should be explored. This process would require test measurements of chamber pressure profiles for promising chamber-propellant configurations but would not require extensive field measurements (except for final selected configurations), since the KA codes appear adequate for estimating the major blast field effects of chamber pressure profile changes.

It would also be desirable to conduct further analytical parametric studies of the effects of chamber pressure profile variations on back-blast pressures, in order to better define what would be the most desirable chamber pressure profiles that could be obtained for various desired muzzle velocities. For example, the present studies have indicated that suitable modification of the initial stages of the chamber pressure profile could greatly reduce field pressures, but not enough cases were considered to furnish detailed guidelines for optimum chamber pressure profile design.

As part of the above recommended analytical studies it would be desirable to include consideration of multiple nozzles of several segments in order to obtain a more optimum gun design than could be obtained by consideration of chamber profile changes alone.

REFERENCES

1. Westine, P.S., and Cox, P.A., 1973: Effects of Breech Blast from a Modified 105-mm Recoilless Rifle on the AH-1G Tail Boom. Final Technical Report under Contract DAAF 07-72-C-0331 for Watervliet Arsenal, Southwest Research Institute.
2. Criscione, E.S., 1971: An Evaluation of the Blast Damage to the UH-1 Helicopter in Event Dial Pack (U). Kaman Avidyne Report KA TM-55. (Confidential Report).
3. Watervliet Arsenal, 1972-1973: Oscillograph Records of Chamber Pressures and field Pressures obtained for Rounds 1, 3, 13, 19 and 48 of the Picatinny Arsenal SEAS 105-mm RR Blast Reduction Tests.
4. Watervliet Arsenal, 1972-1973: SWEVW-RDD-SE Letters and Memorandums on SEAS 105-mm RR Blast Reduction Tests, dated 4 December 1972, 19 December 1972, 8 March 1973, 1 May 1973 and 3 July 1973.
5. Lemcke, B., 1964: On the Use of Artificial Viscosity in Finite-Difference Calculations of Nonuniform Unsteady One-Dimensional Flow. ASRL TR 126-1, Massachusetts Institute of Technology.
6. Godunov, S.K., 1959: A Difference Method for Numerical Calculation of Discontinuous Solution of the Equations of Hydrodynamics, Mat. Sb. 47, p. 271-306.
7. Thompson, J.H., and Ruetenik, J.R., 1971: Computer Code for Ground-Reflected Blast Wave, Kaman Avidyne Report KA TR-79.
8. Ruetenik, J.R., 1973: Analysis of Godunov Method with Fixed Mesh for Hydrodynamic Calculations, Sponsored by Kaman Avidyne Internal Research and Development Program, Proprietary.

TABLE 1

POSITIONS ON THE AH-1G TAIL BOOM
(All in Inches)

Position (See Figure 1)	A (Critical)	B (Rear)	C (Tip)
Downstream distance from standard nozzle exit (x)	95	241	312
Lateral distance from nozzle centerline	48	54	60
Helicopter Boom Station	70	216	287

TABLE 2

COMPARISON OF EXPERIMENTAL AND CALCULATED FIELD OVERPRESSURES

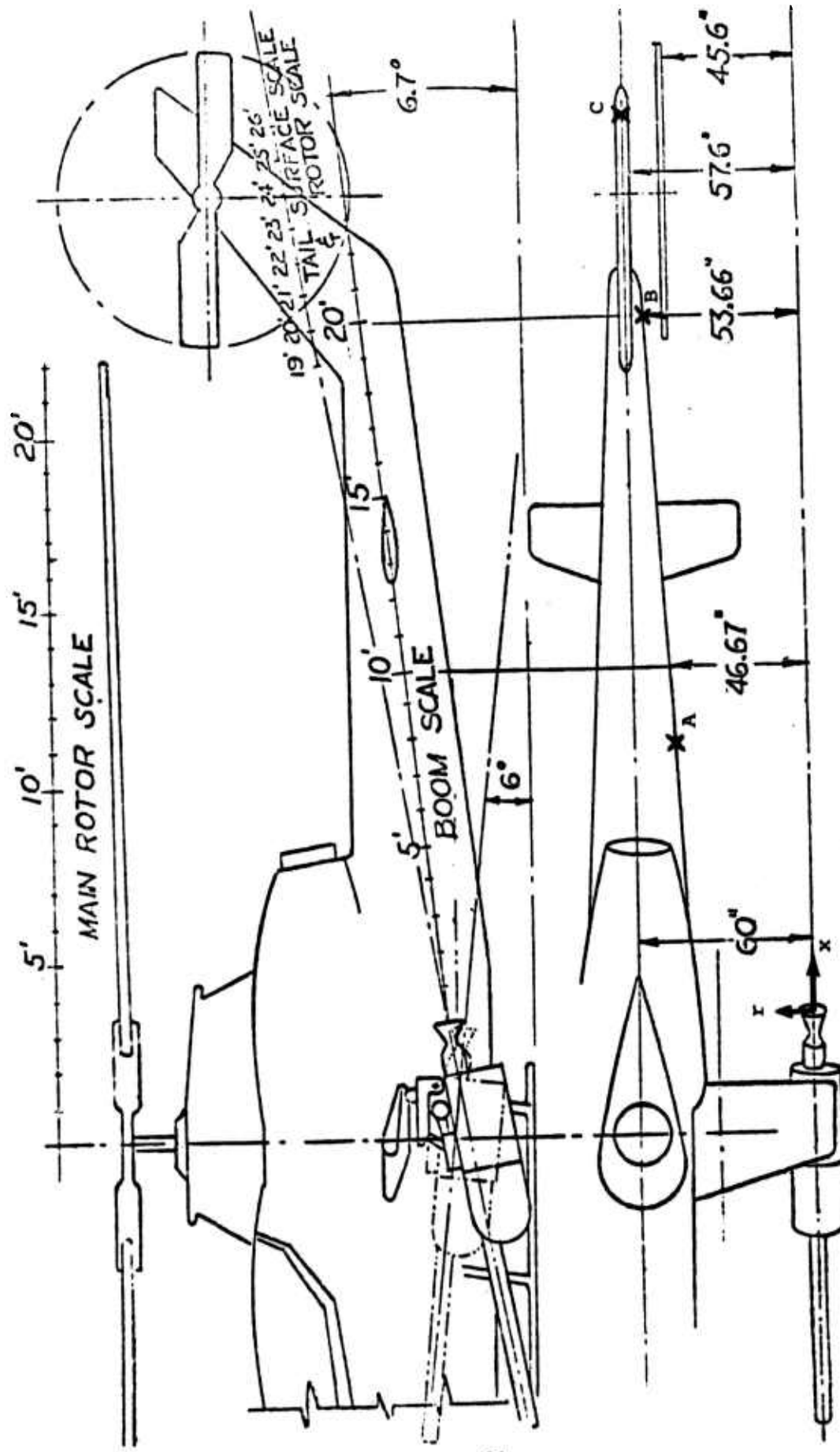
Round	Position (in.) (see Fig. 1)		Peak Field Overpressure (psi)			
	x	r	Free-Field		Reflected	
			Exper.	Calc.*	Exper.	Calc.*
1	60	60	11.4	3.1	-----	-----
	104	60	4.7	4.6	-----	-----
	224	60	3.7	5.6	-----	-----
3	60	35	14.3	4.3	-----	-----
	60	60	6.6	2.6	-----	-----
	104	60	12.9	3.8	-----	-----
13	12	48	-----	-----	1.7	2.4(2.1)
	24	48	-----	-----	2.8	3.2(3.0)
	48	48	-----	-----	3.2	4.4(4.4)
	83	48	4.5	3.1(3.0)	9.4	6.7(6.6)
	179	48	9.0	5.6(6.0)	19.5**	12.8(13.9)
48	48	48	-----	-----	2.6	3.0
	83	48	3.5	2.2	-----	-----
	115	48	-----	-----	11	6.1
	147	48	-----	-----	6,11	8.4
	179	48	7	4.4	2.7	9.9

* Values in () are for an axial grid spacing about half that of the other values
 ** Questionable value.

TABLE 3
CONDITIONS AND RESULTS OF PARAMETRIC STUDIES

Profile*	Figure	Peak Chamber Pressure (psi)	Time of Pk. Chamber Pressure (ms)	Muzzle Velocity (fps)	Peak Field Reflected Over-pressure (psi) at Position:		
					A	B	C
1	8	8500	5.90	850	6.4	13.2	13.4
2	8	5750	6.36	850	5.2	10.8	10.5
3	8	4400	7.20	850	4.9	10.2	10.4
4	8	3150	8.04	850	3.8	8.4	8.7
4A	11	3150	12.04	900	2.1	6.4	7.4
4B	11	3150	18.04	900	1.9	1.9	3.7
1		8500	5.90	850	6.4	13.3	13.4
5	10	8500	7.90	1005	5.5	11.3	11.3
6		8500	9.90	1135	4.5	9.8	9.8
2		5750	6.36	850	5.2	10.8	10.5
7	12	5750	6.36	1020	5.2	10.8	10.5
8		5750	6.36	1100	5.2	10.8	10.5
1'	*	18500	5.90	1800	10.7	22.8	25.6
2'	9	6800	6.36	1000	5.8	11.5	11.9
2''	9	12800	6.36	1800	8.4	16.9	18.4
10		3720	2.15	-	7.8	10.2	-
Round 1	13	7450	3.70	500	10.0	13.6	-

* Profiles designated by primes are essentially the same shape as the corresponding (unprimed) profiles in Figure 8, except that all pressures are proportionally higher according to the ratio of peak chamber pressures indicated in this table.



(U) Figure 1. AH-1G Helicopter Geometry

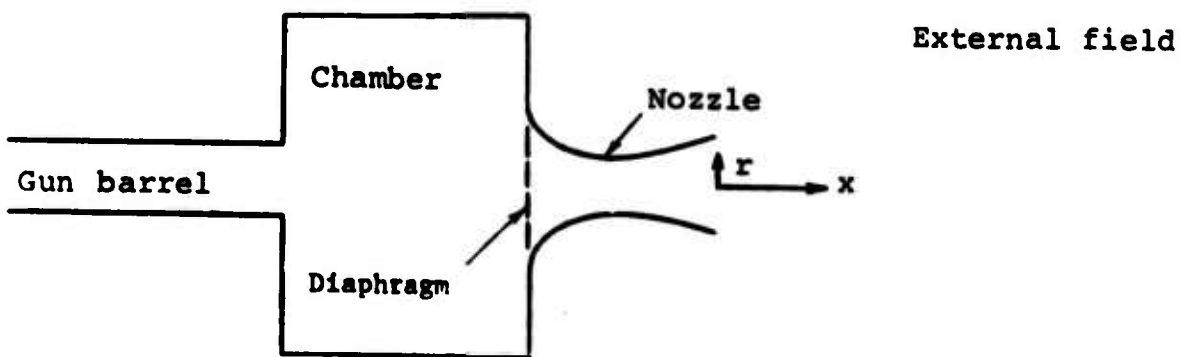


Figure 2. Overall Blast Field Problem

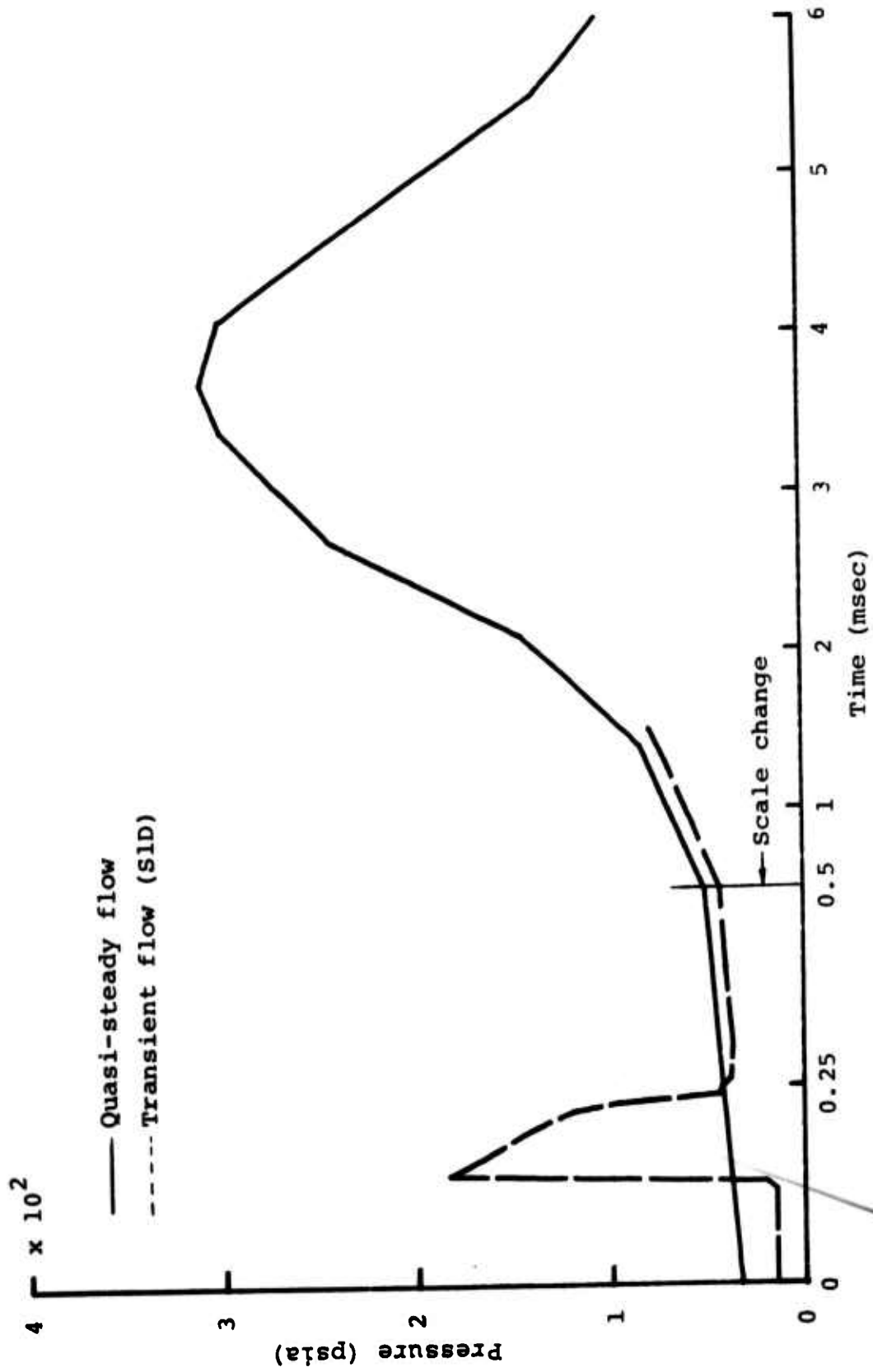


Figure 3. - Comparison of Computed Nozzle Exit Pressures for Transient and Quasi-Steady Flow

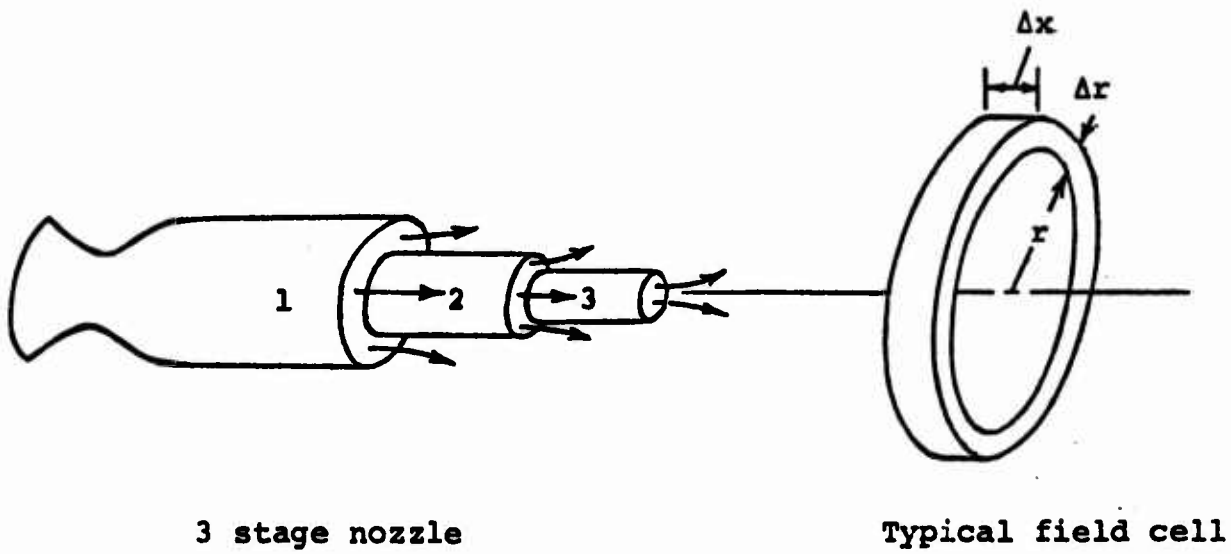


Figure 4. Nozzle and External Flow Representation

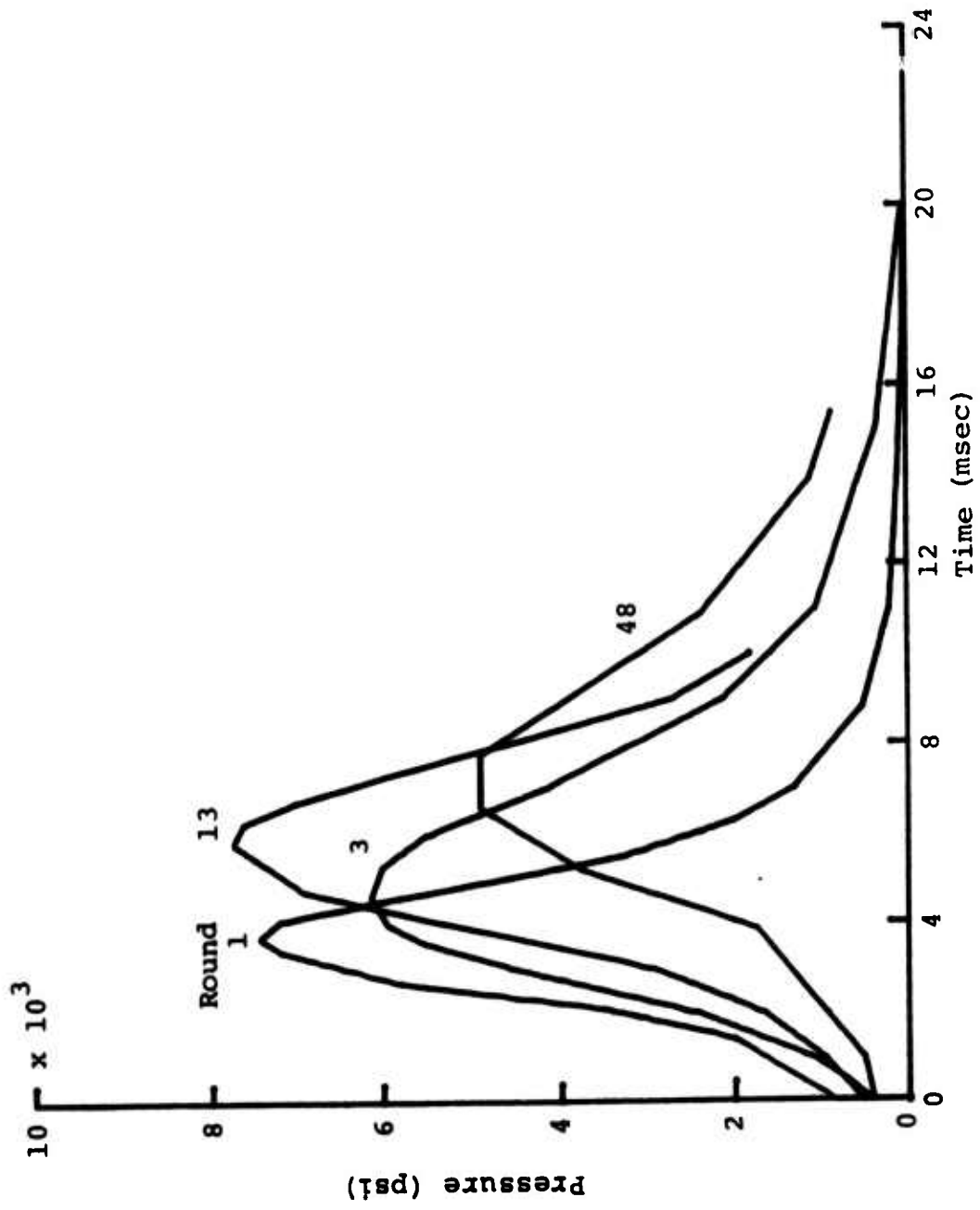
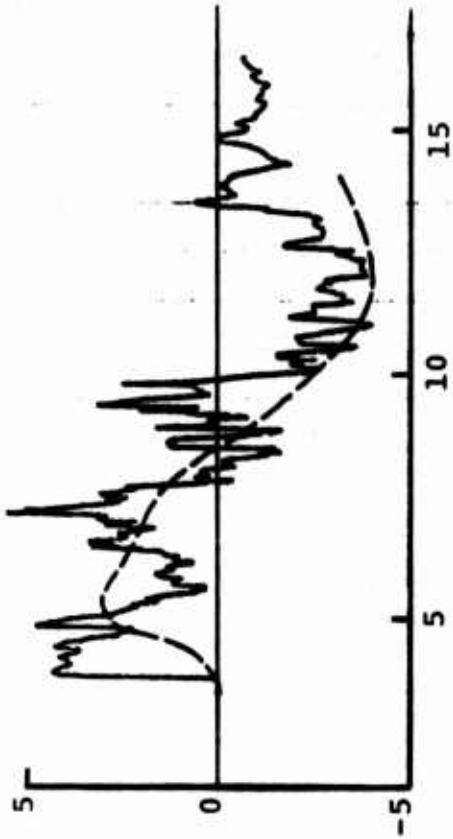


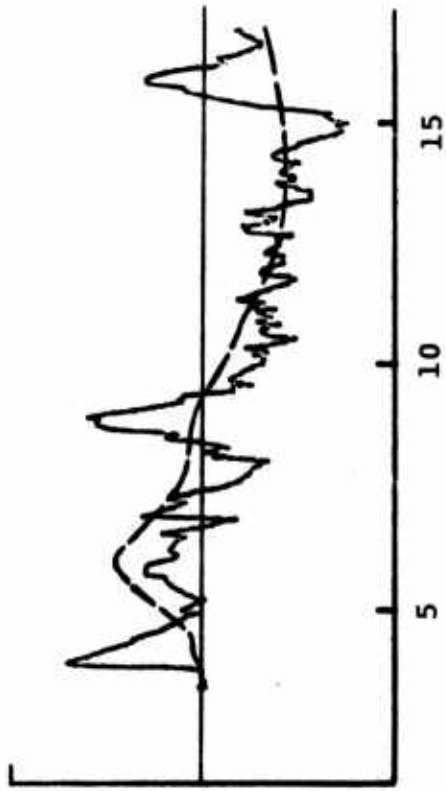
Figure 5. Chamber Pressure Profiles of Picatinny Tests

Round 13

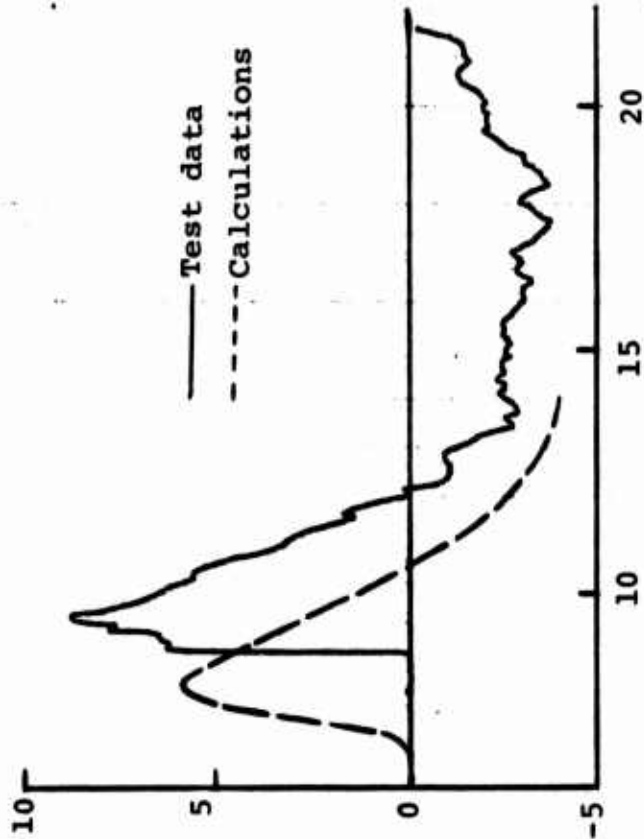


x = 83"

Round 48



-96-



x = 179"

Time (msec)

Figure 6. Experimental and Calculated Free-Field Overpressure Time Histories at Two Stations 48 inches from the Gun Axis

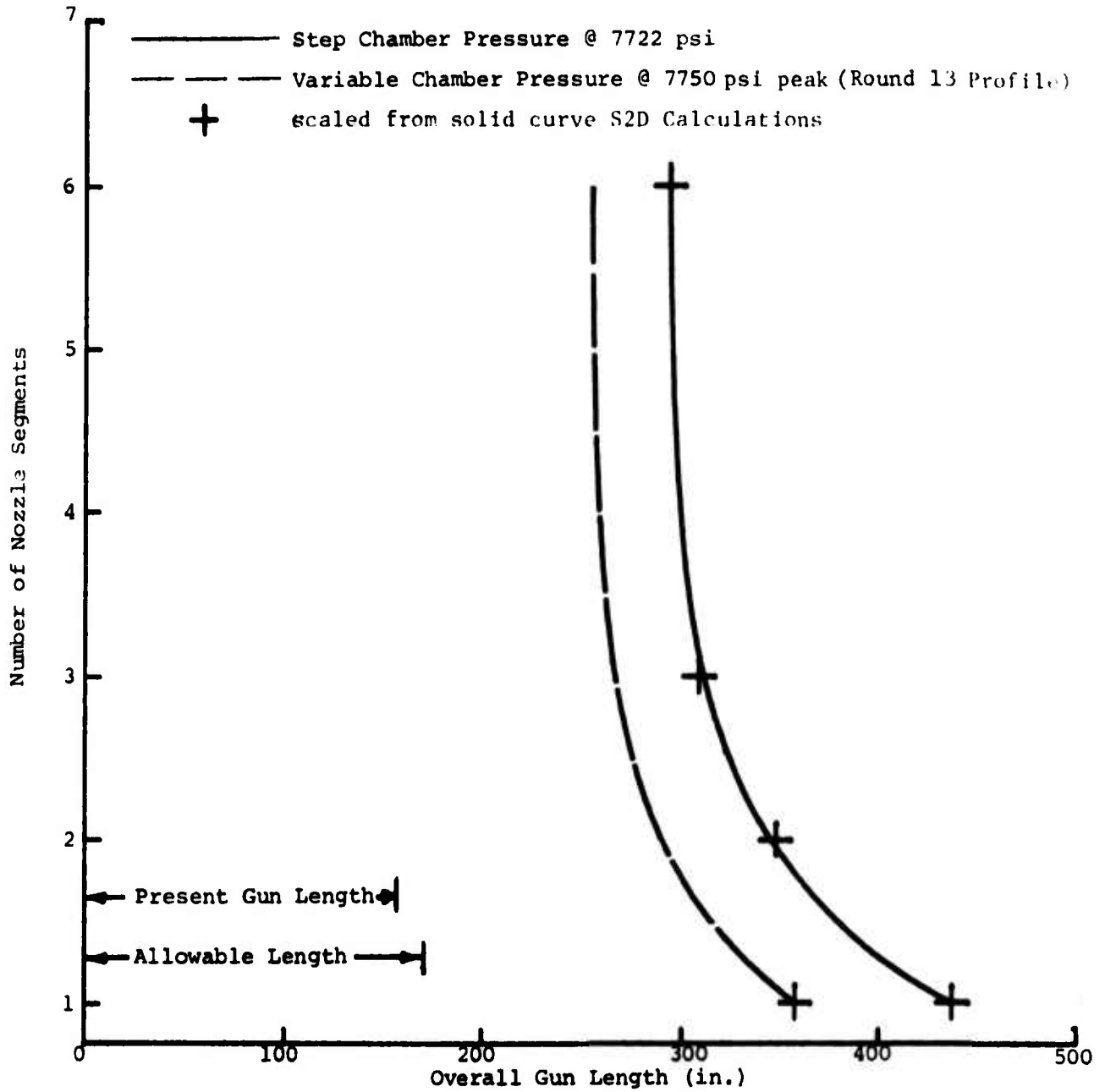


Figure 7 - Gun Length Needed with a Multiple Nozzle to Reduce Reflected Overpressure to 5 psi at 60 inches from Gun Axis

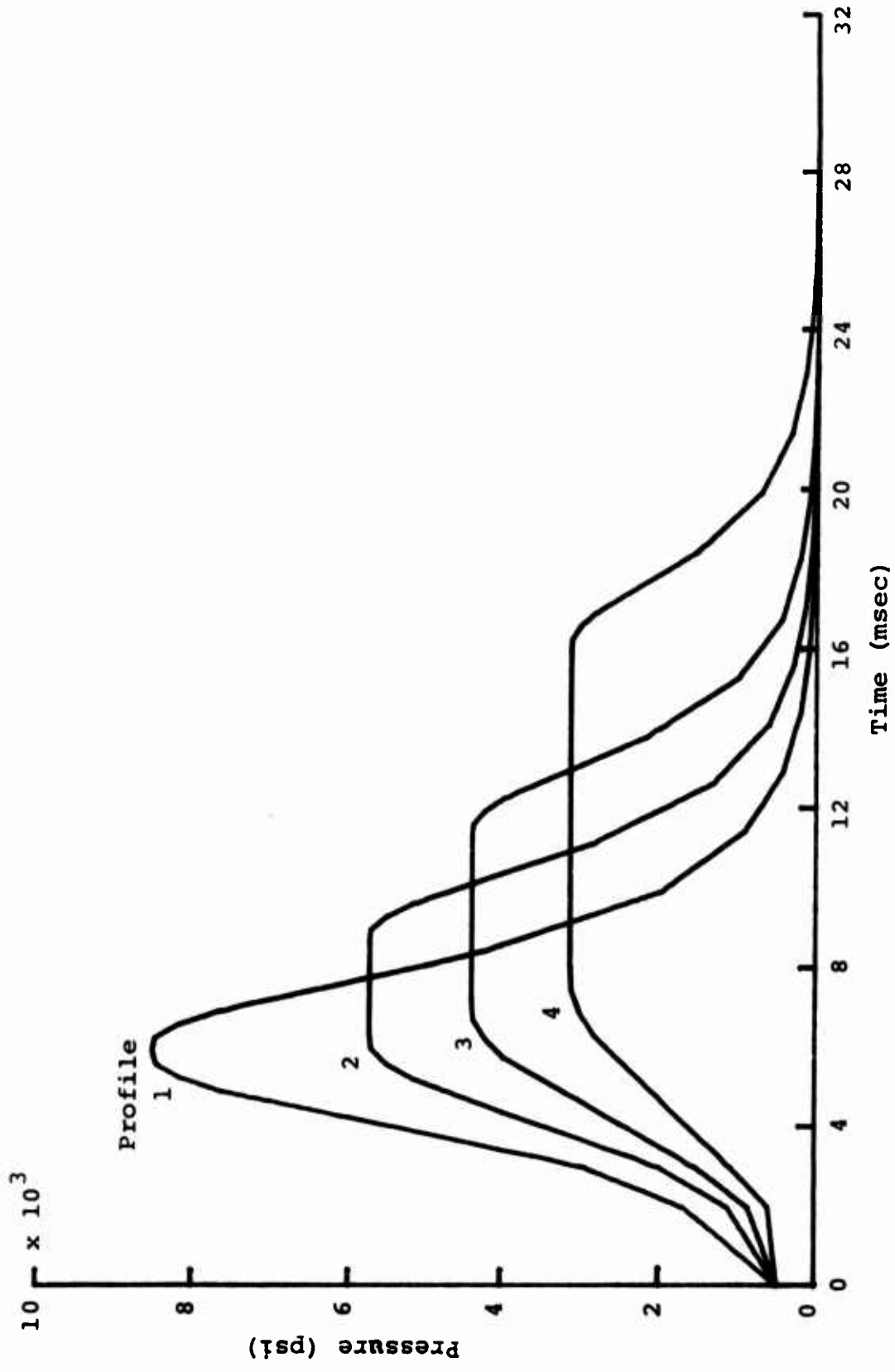


Figure 8. Chamber Pressure Profiles for Peak Pressure Studies for Constant Muzzle Velocity

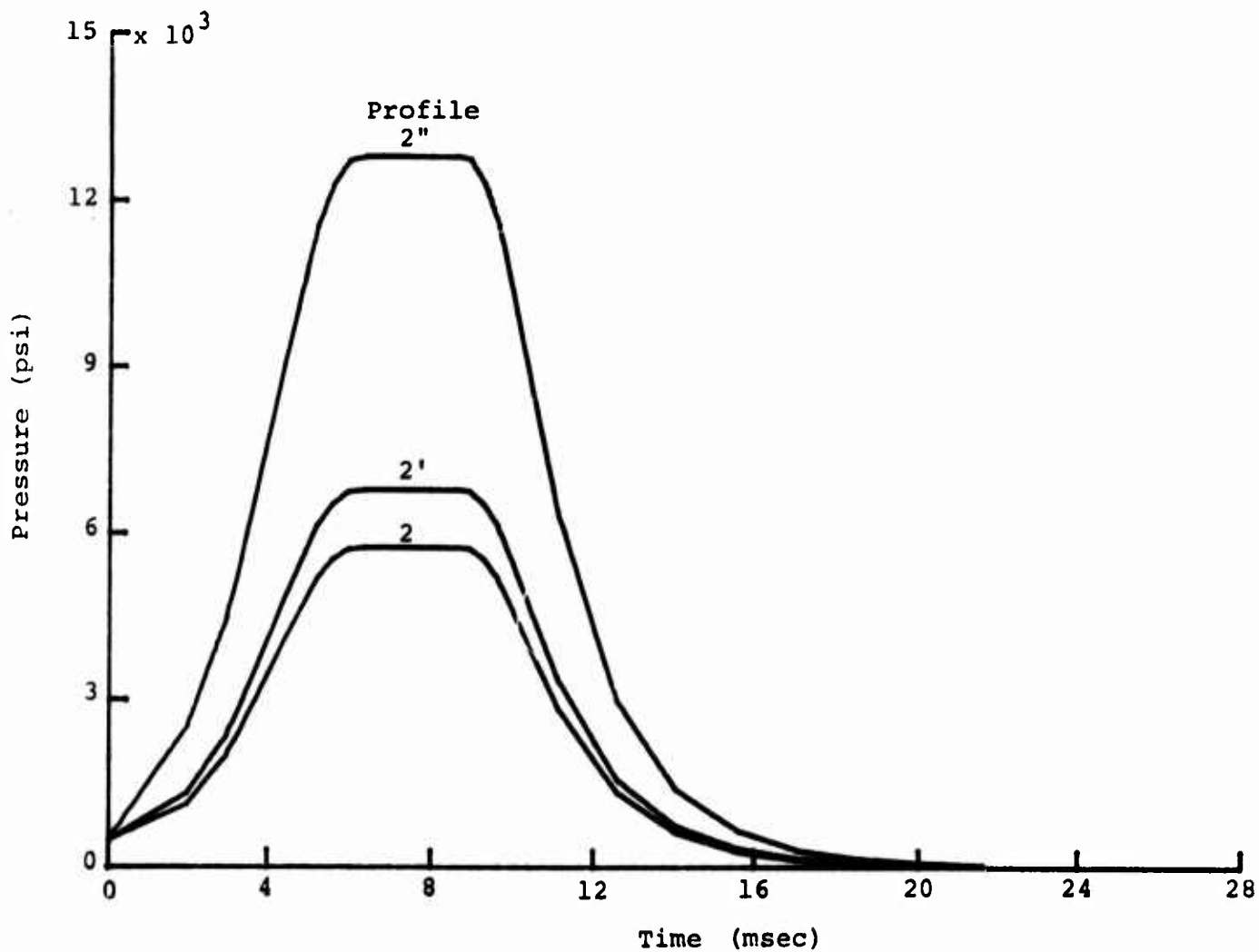


Figure 9. Chamber Pressure Profile Family 2 for Peak Pressure Studies with a Single Profile Shape

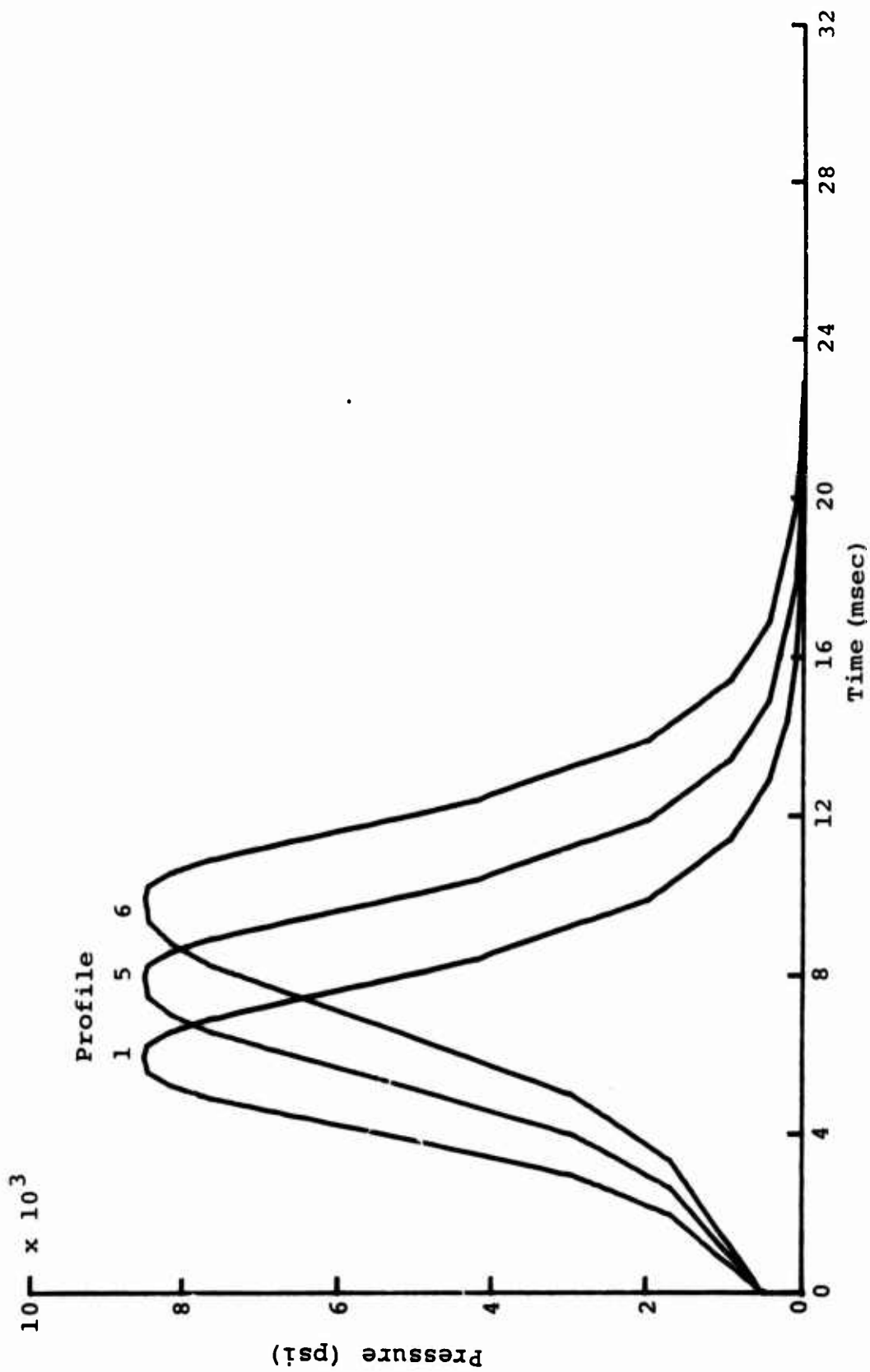


Figure 10. Chamber Pressure Profiles for Rise Rate Studies

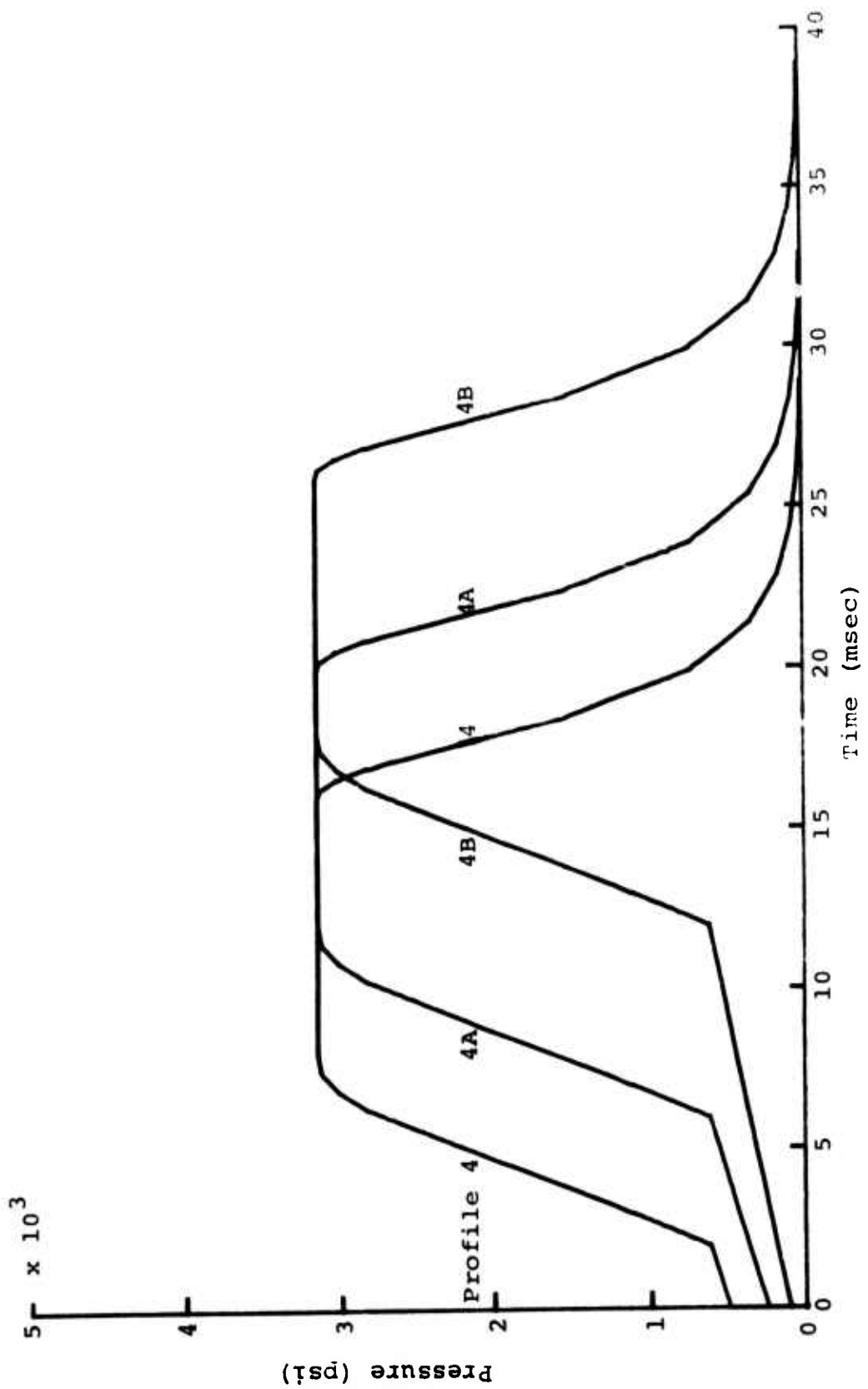


Figure 11. Chamber Pressure Profiles for Initial Buildup Studies

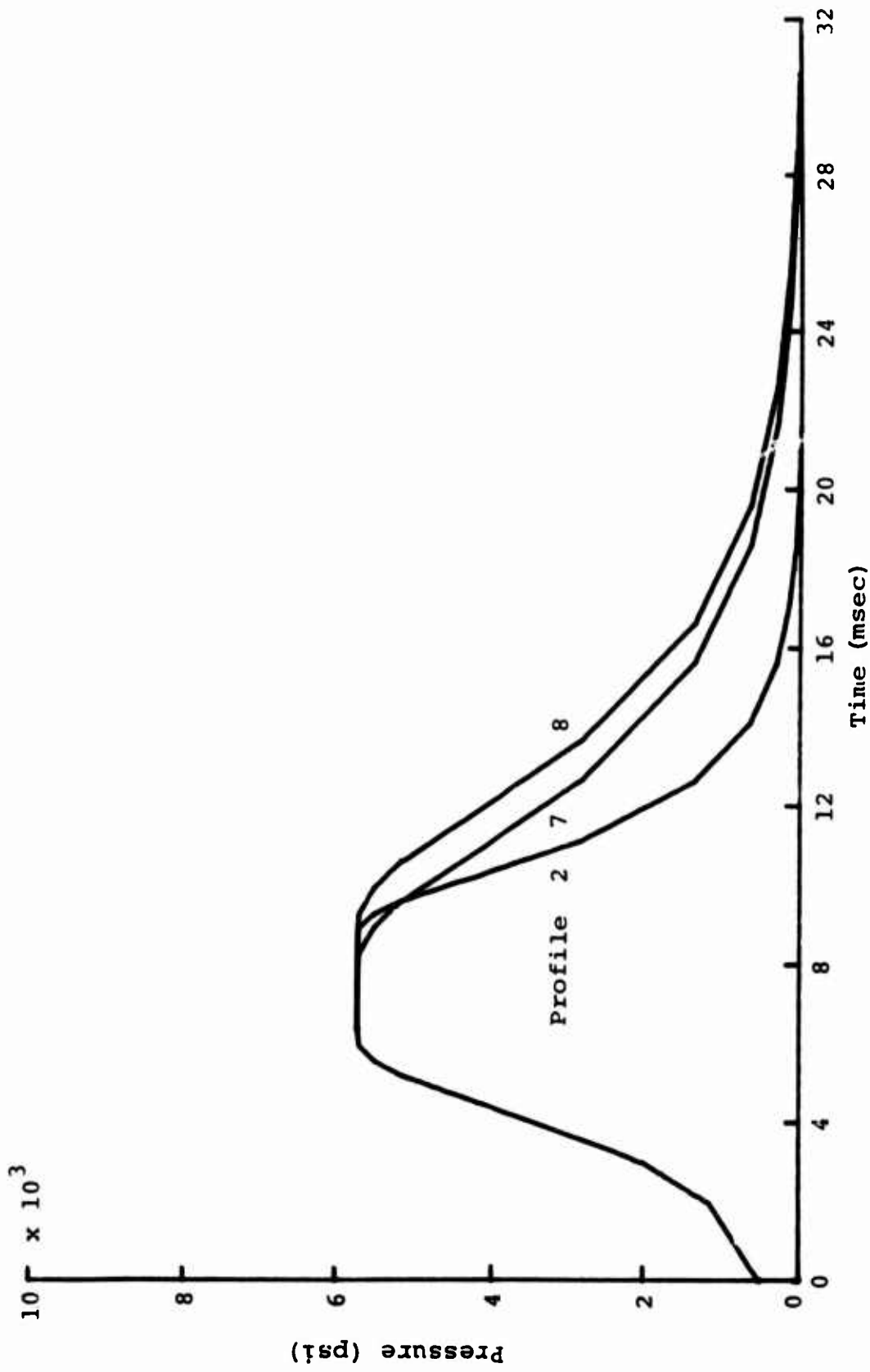


Figure 12 . Chamber Pressure Profiles for Decay Shape Studies

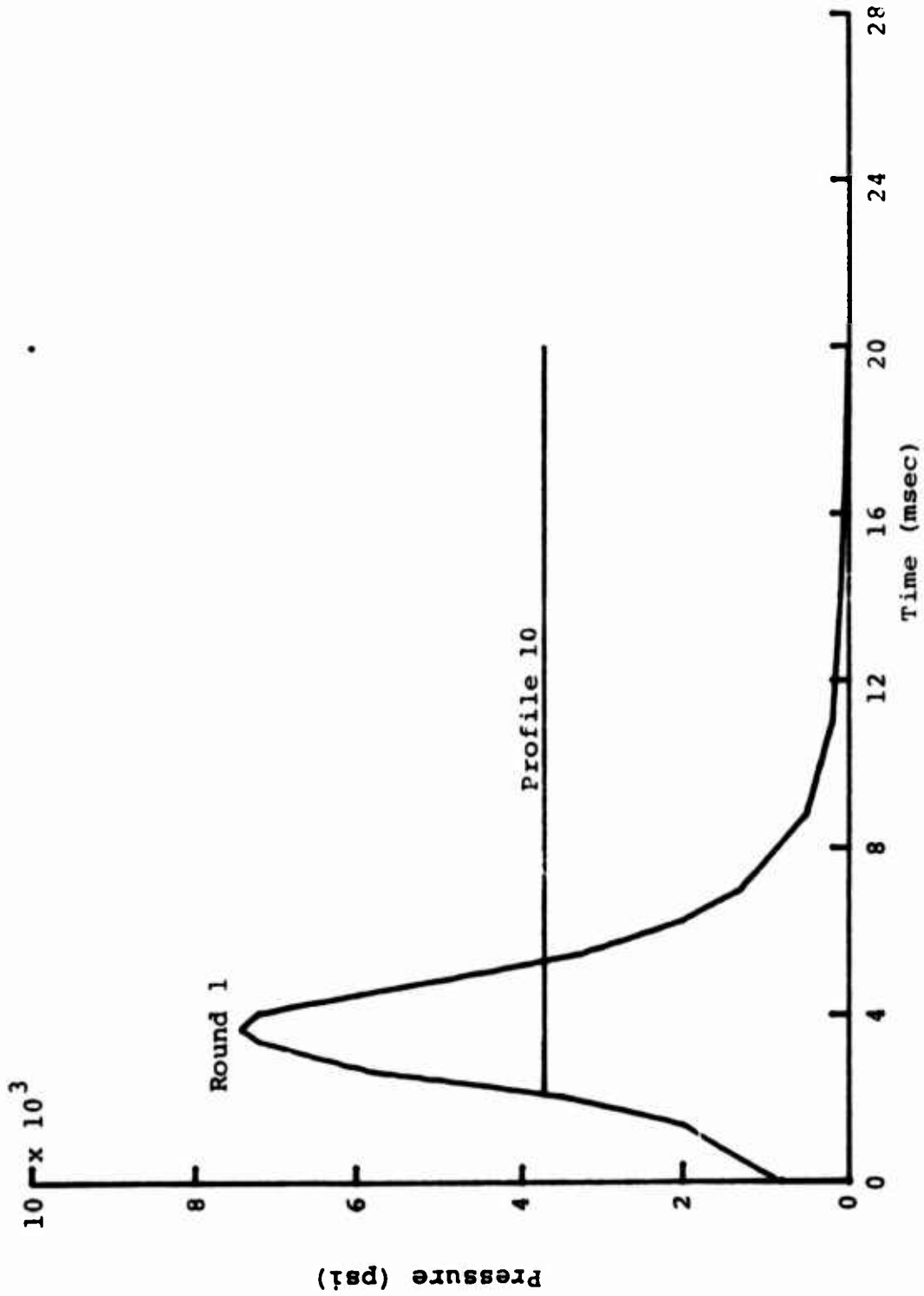


Figure 13. Two Chamber Pressure Profiles for Short Times to Peak Pressure

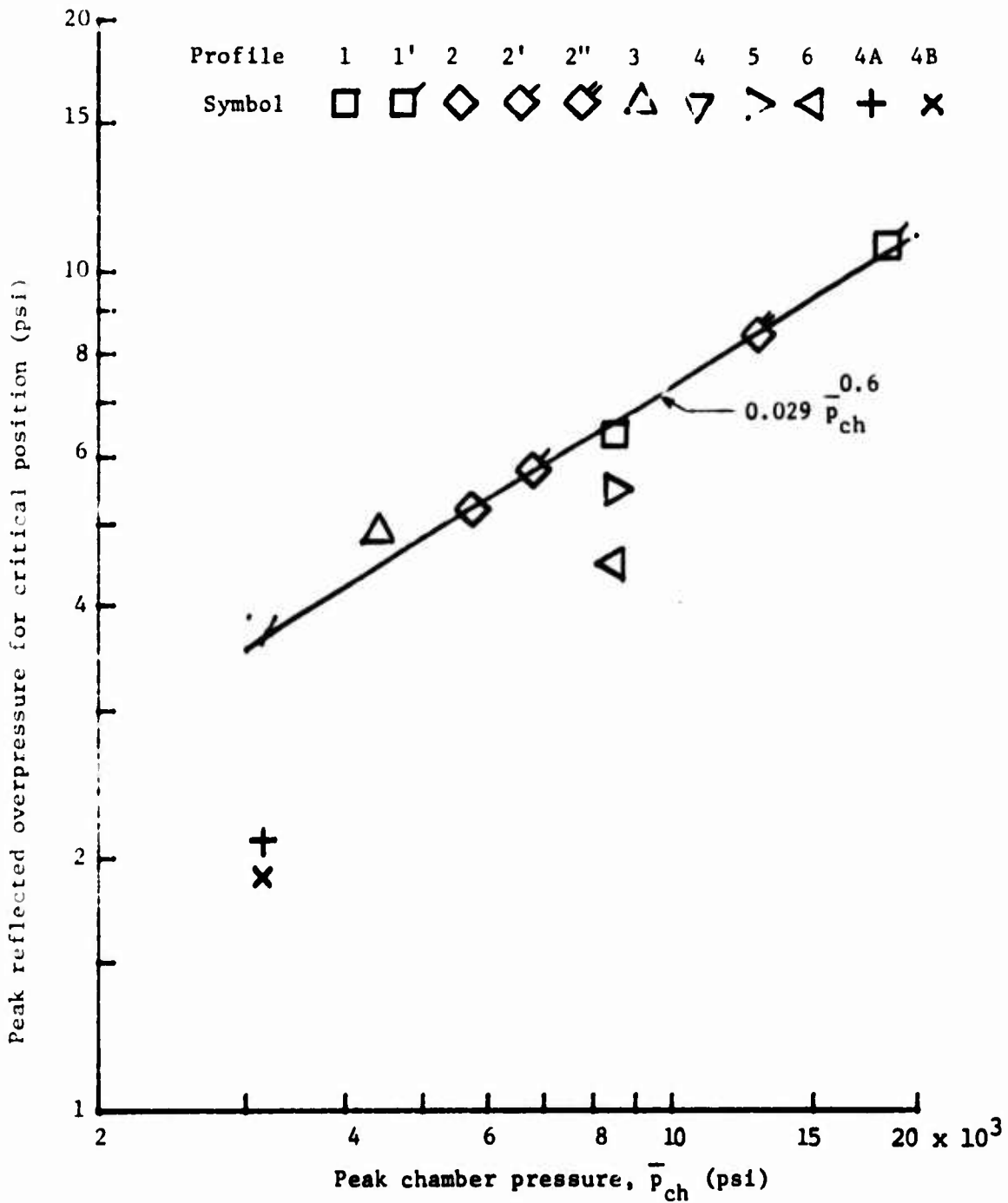


Figure 14. Effect of Peak Chamber Pressure on Peak Reflected Pressure

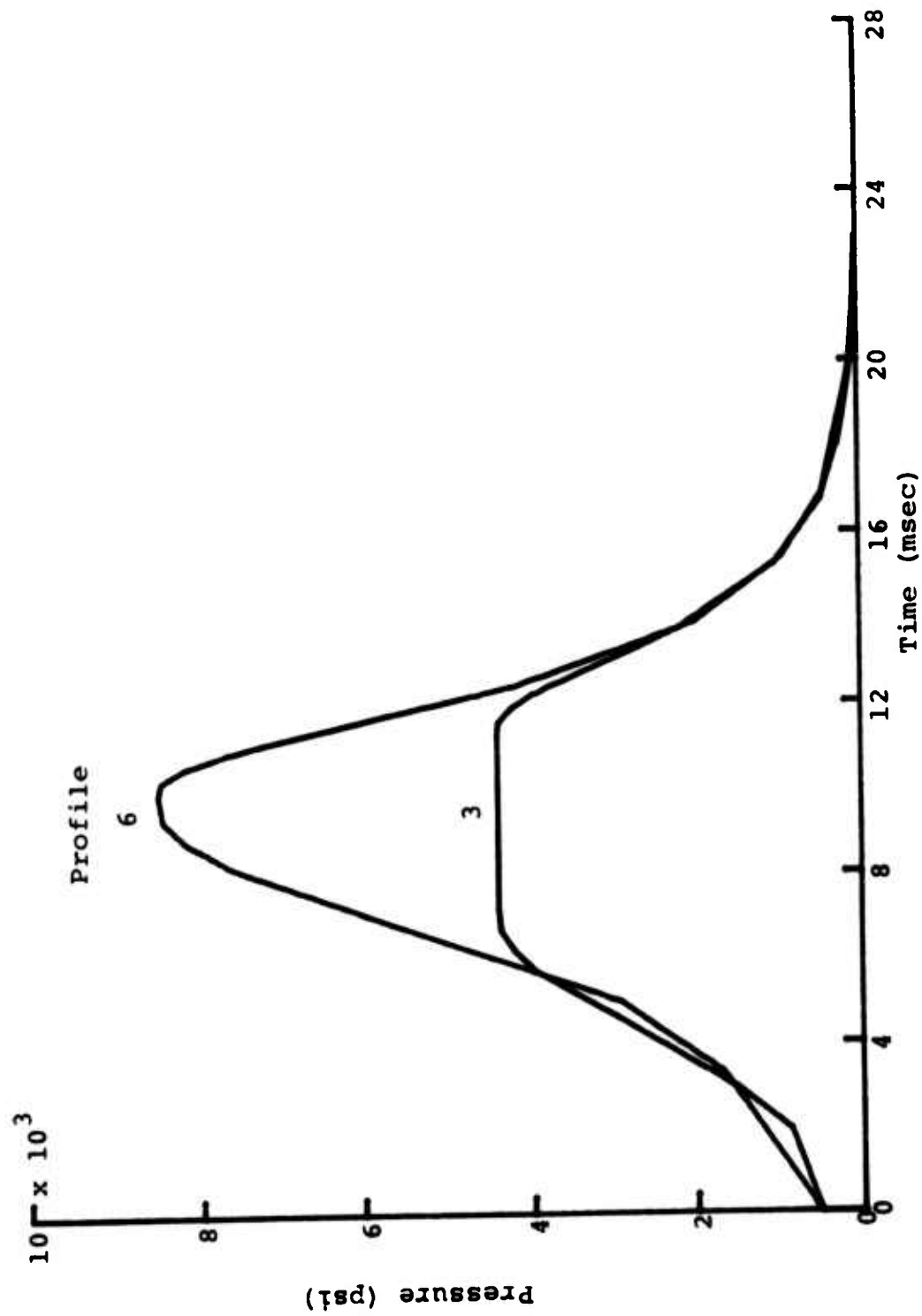


Figure 15 . Comparison of Chamber Pressure Profiles 3 and 6

Position A

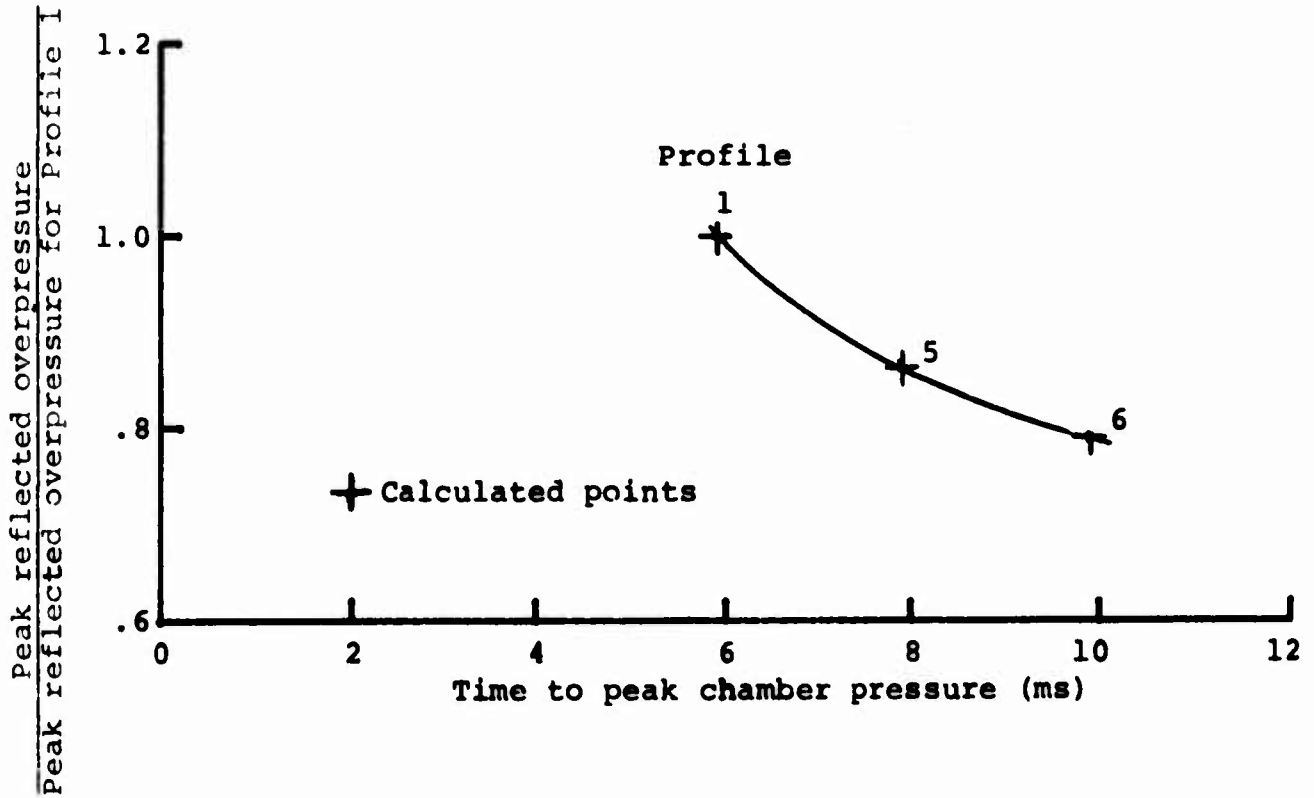


Figure 16. Effect of Chamber Pressure Rise Rate on Reflected Pressure (Profiles of Fig. 10)

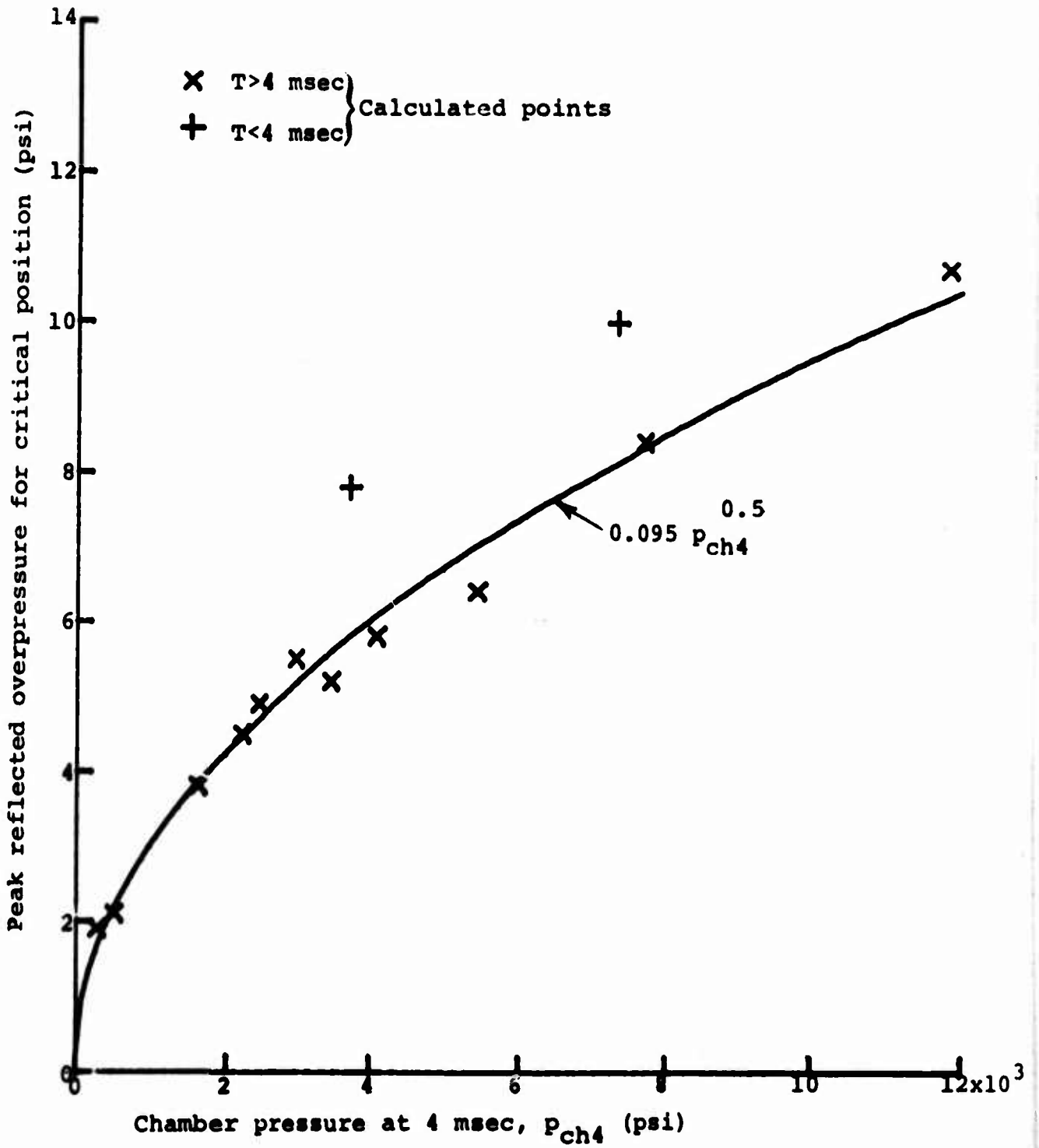


Figure 17. Variation of Peak Reflected Pressure with Chamber Pressure at 4 msec.

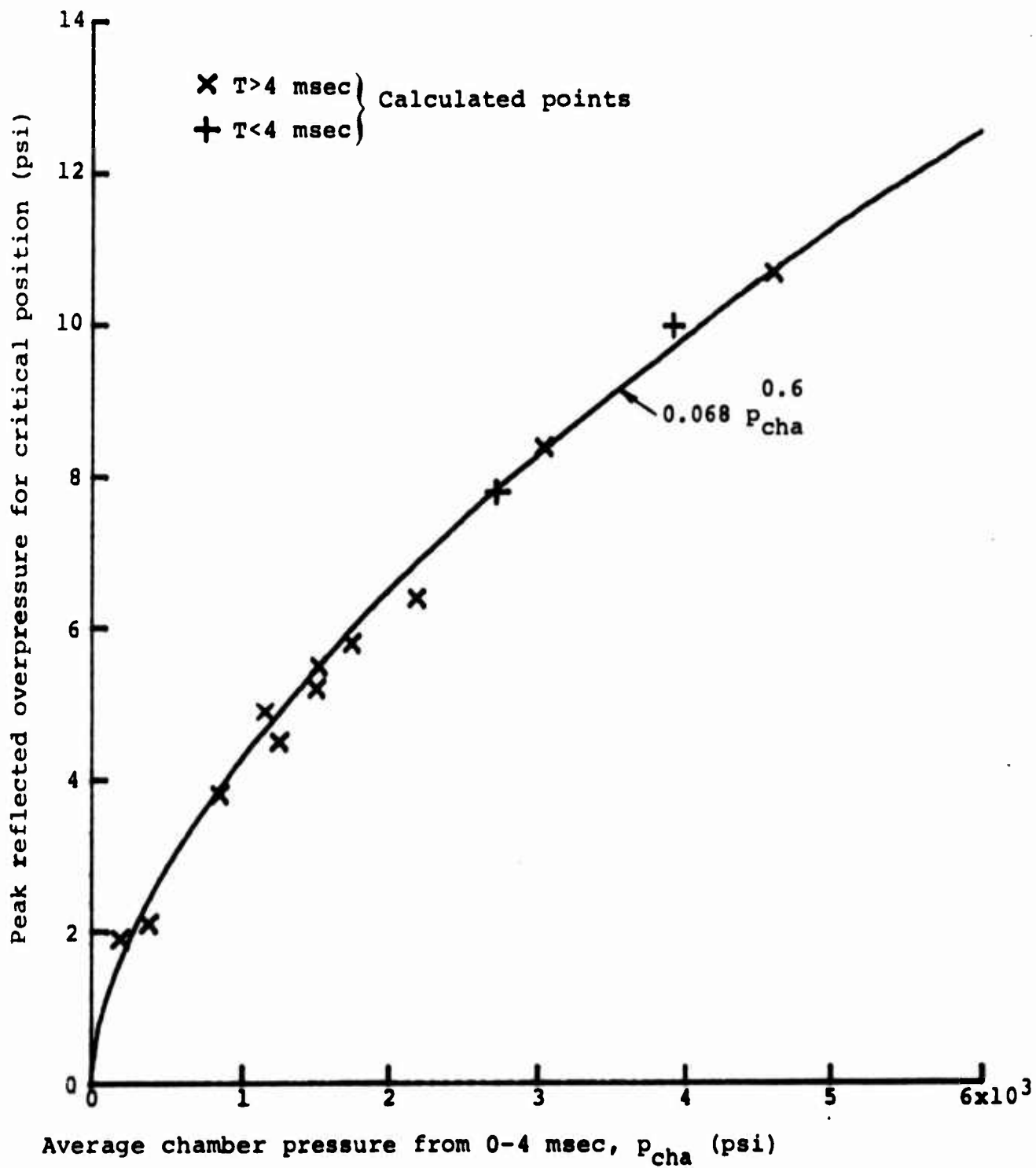


Figure 18. Variation of Peak Reflected Pressure with Average Chamber Pressure from 0-4 msec.

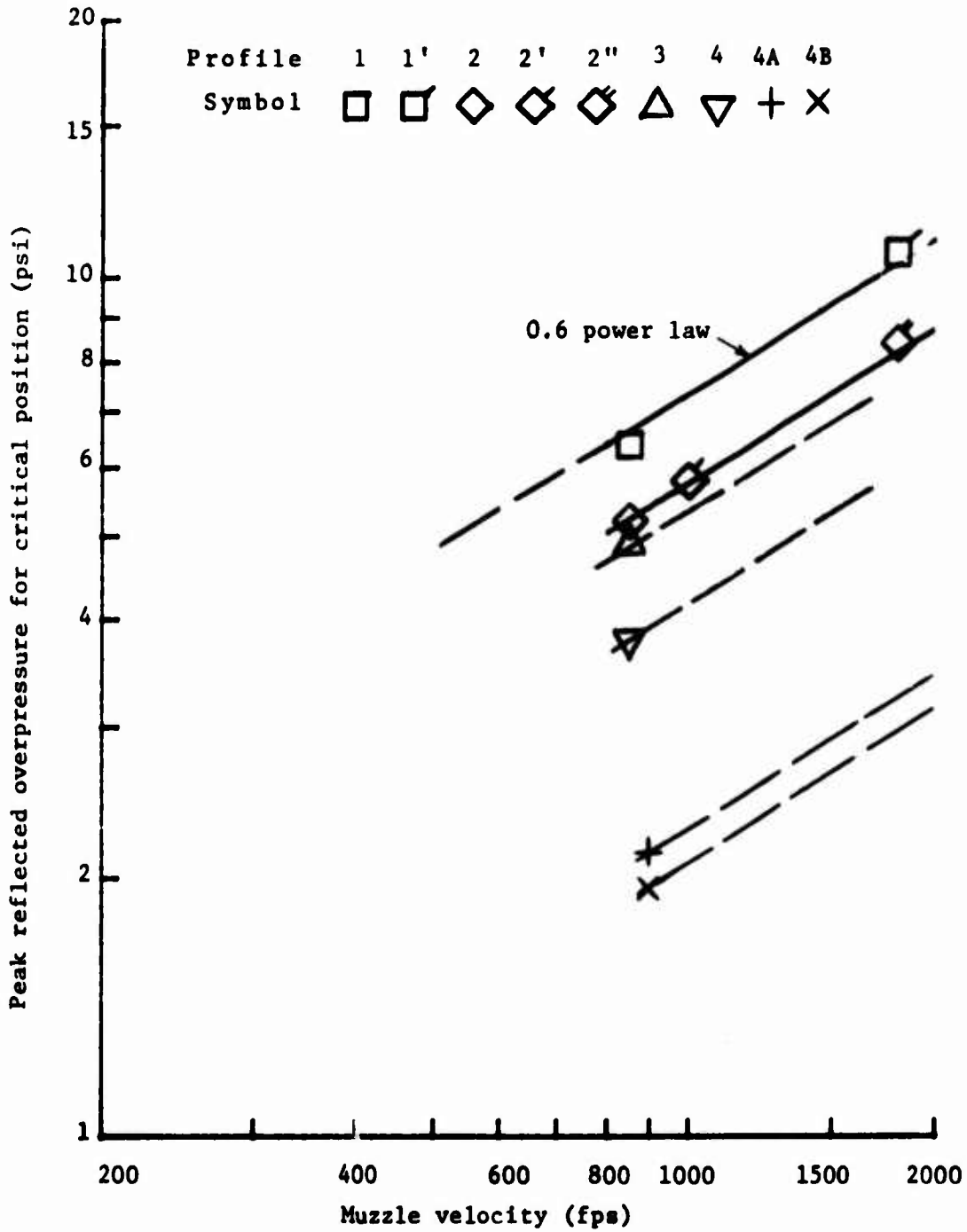


Figure 19. Variation of Peak Reflected Pressure with Muzzle Velocity for a 25-Pound Projectile

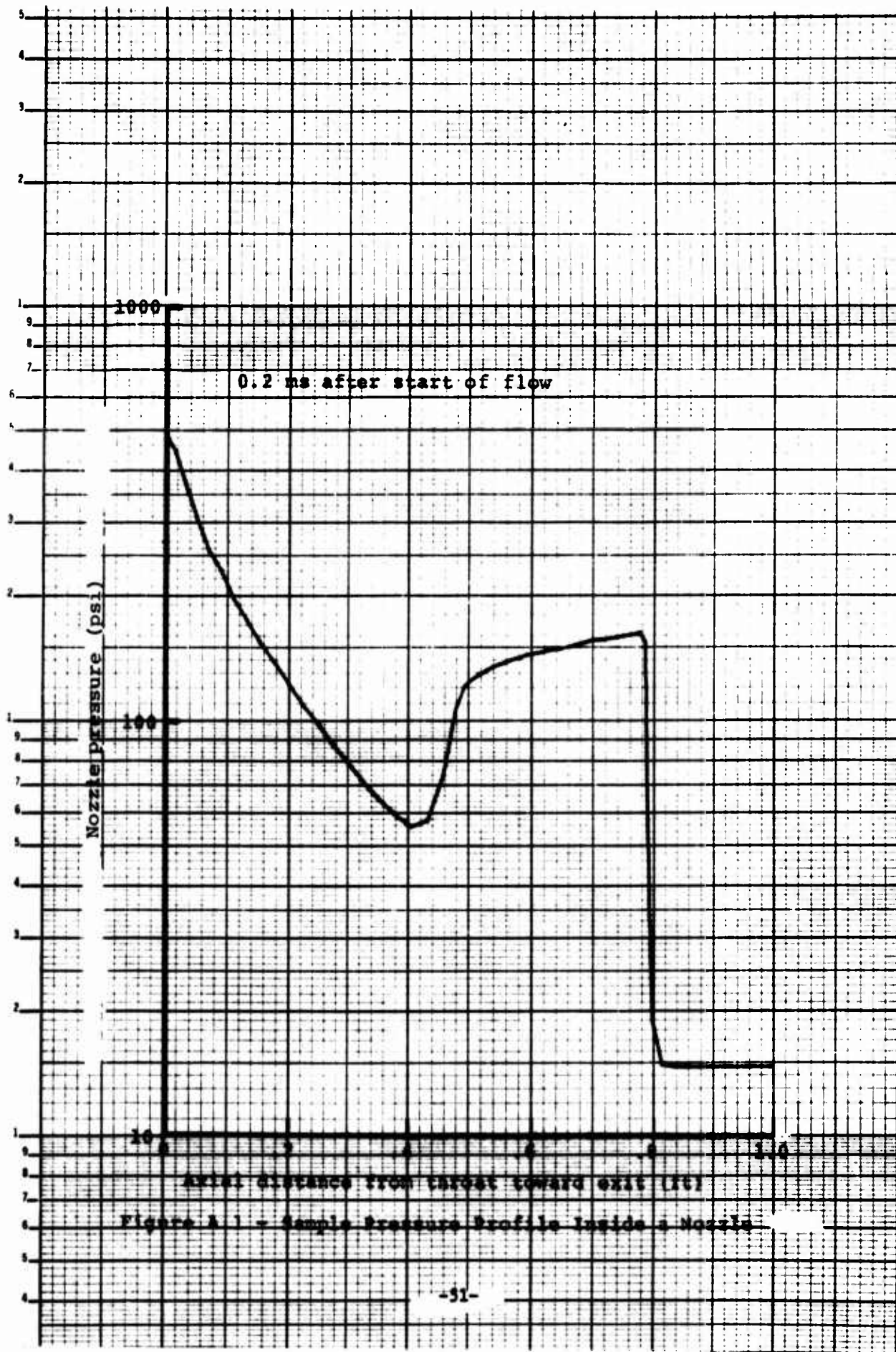
APPENDIX A

S1D CODE

The S1D computer code was developed to solve the problem of unsteady non-uniform one-dimensional sonic-throat flow through a convergent-divergent nozzle of arbitrary variable cross section. For the convergent section of the nozzle, the flow is assumed to be quasi-steady with sonic velocity at the throat. For the divergent section, the flow process is calculated by an extension of the numerical finite-difference procedure of Reference 5.

The S1D computer code receives as inputs time histories of chamber pressure and density and provides as outputs time histories of exit pressures, densities and velocities and also provides profiles of internal nozzle pressure distributions at selected times.

A sample time history of nozzle exit pressure obtained from the S1D code is shown by the dashed line in Figure 3, and a sample pressure profile inside a nozzle is given in Figure A.1. The latter figure applies to a time shortly after flow initiation (0.2 ms), where the flow has not yet had time to reach the nozzle exit. Figure A.1 indicates a nearly quasi-steady pressure decay for short distances from the throat of the nozzle (less than 0.4 ft), a shock structure moving toward the nozzle exit for intermediate distances (0.4 - 0.8 ft), and undisturbed air at atmospheric pressure near the nozzle exit (>0.8 ft).



APPENDIX B

S2D CODE

The S2D computer code was developed to solve the axially-symmetrical external flow problem of the exit of a prescribed flow (with arbitrary time histories of exit pressure, density and velocity) from a set of coaxial nozzles (see Figure 4) into an initially undisturbed atmosphere.

The code computes the flow in a cell system similar to the one shown in Figure B.1. The cells are taken axisymmetric about the nozzle axis, as shown in the figure, so each cell is a ring having a rectangular cross section. The flow from cell to cell is computed using the Godunov technique (Ref. 6), which has been employed in nuclear blast-field calculations by Thompson and Ruetenik (Ref. 7).

It should be mentioned, however, that Thompson and Ruetenik (Ref. 7) use a moving cell system with the cells so configured that shock waves in the problem fall along cell boundaries. With this scheme the shocks are computed using the Rankine-Hugoniot equations. However, the method is done at the expense of considerable complexity in the formulation of the computer program due to the moving cell system.

For the present problem a fixed cell system has been employed, as described. The effect on the pressure field of using fixed cells was studied by Ruetenik (Ref. 8) for several simple one-dimensional problems. The principal effect of the fixed mesh was found to be that shocks become compression waves having the pressure rise take place over a distance of a few cells. From this study, it was concluded that satisfactory accuracy could be expected for the back-blast problem using the more readily programmed fixed mesh.

Returning to the cell layout of Figure B.1, the input flow to the cell field comes from the exit of the nozzle at the cell boundaries corresponding to nozzle exit. This flow is computed using the chamber conditions and steady-state nozzle flow equations. The solid boundaries of the nozzle are represented by impenetrable cell boundaries. At the outer boundaries of the cell system the boundary condition of no reflection is used.

Output from the S2D computer code is available in a variety of options, ranging from selected tables of field pressures, densities and velocities to three-dimensional plots of the pressure field.

One of the most convenient output forms is a map of the maximum or peak pressure reached at every point (cell) in the external flow field. A sample printout is shown in Figure B.2. This same information can also be presented in a pictorial three-dimensional form, as is indicated in Figure B.3 for a three-stage multiple nozzle situation. Locations of the three nozzle segments in this figure are designated by the three solid bars numbered 1, 2, 3 at the top of the figure, and all pressure values over 30 psi have been truncated to 30 psi to keep the figure to a tolerable size.

Similar plots to Figures B.2 and B.3 can also be printed out for the instantaneous pressure fields at any selected times.

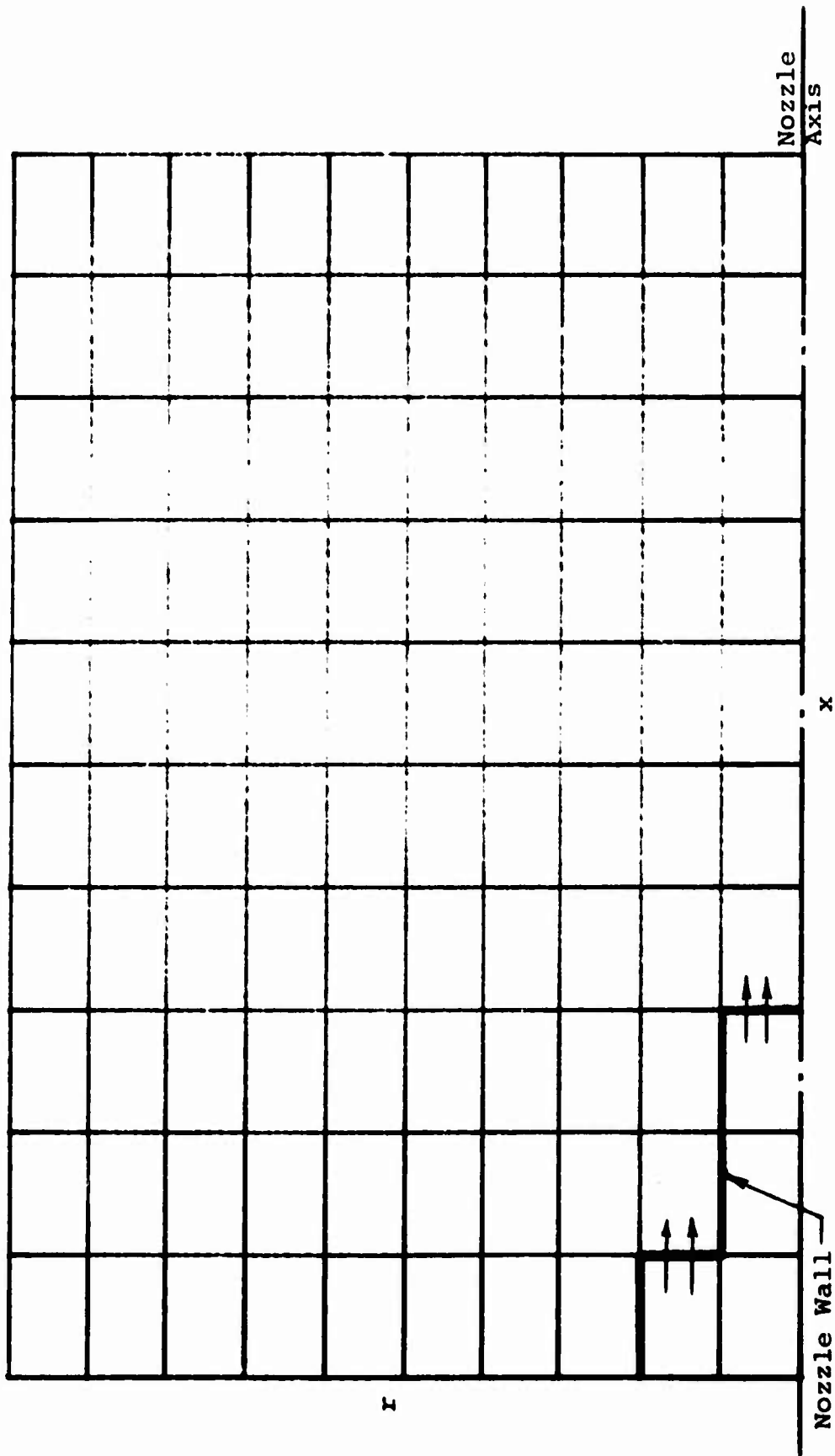


Figure B.1 Cell Layout Employed in S2D Code for Computing the Back-Flast Pressure Field

		r(in)															
		0	10	20	30	40	50										
ACCUMULATED MAXIMUM (OVER) PRESSURES, IN TENTHS OF PSI																	
Cell	→	1	2	3	4	5	6	7	8	9	10	11	12	13	14	15	16
0	1	1.16	1.2	1.3	1.4	1.5	1.6	1.7	1.8	1.9	2.0	2.1	2.2	2.3	2.4	2.5	2.6
0	2	1.15	1.2	1.3	1.4	1.5	1.6	1.7	1.8	1.9	2.0	2.1	2.2	2.3	2.4	2.5	2.6
0	3	1.15	1.2	1.3	1.4	1.5	1.6	1.7	1.8	1.9	2.0	2.1	2.2	2.3	2.4	2.5	2.6
0	4	1.15	1.2	1.3	1.4	1.5	1.6	1.7	1.8	1.9	2.0	2.1	2.2	2.3	2.4	2.5	2.6
0	5	1.15	1.2	1.3	1.4	1.5	1.6	1.7	1.8	1.9	2.0	2.1	2.2	2.3	2.4	2.5	2.6
0	6	1.15	1.2	1.3	1.4	1.5	1.6	1.7	1.8	1.9	2.0	2.1	2.2	2.3	2.4	2.5	2.6
0	7	1.15	1.2	1.3	1.4	1.5	1.6	1.7	1.8	1.9	2.0	2.1	2.2	2.3	2.4	2.5	2.6
0	8	1.15	1.2	1.3	1.4	1.5	1.6	1.7	1.8	1.9	2.0	2.1	2.2	2.3	2.4	2.5	2.6
0	9	1.15	1.2	1.3	1.4	1.5	1.6	1.7	1.8	1.9	2.0	2.1	2.2	2.3	2.4	2.5	2.6
0	10	1.15	1.2	1.3	1.4	1.5	1.6	1.7	1.8	1.9	2.0	2.1	2.2	2.3	2.4	2.5	2.6
0	11	1.15	1.2	1.3	1.4	1.5	1.6	1.7	1.8	1.9	2.0	2.1	2.2	2.3	2.4	2.5	2.6
0	12	1.15	1.2	1.3	1.4	1.5	1.6	1.7	1.8	1.9	2.0	2.1	2.2	2.3	2.4	2.5	2.6
0	13	1.15	1.2	1.3	1.4	1.5	1.6	1.7	1.8	1.9	2.0	2.1	2.2	2.3	2.4	2.5	2.6
0	14	1.15	1.2	1.3	1.4	1.5	1.6	1.7	1.8	1.9	2.0	2.1	2.2	2.3	2.4	2.5	2.6
0	15	1.15	1.2	1.3	1.4	1.5	1.6	1.7	1.8	1.9	2.0	2.1	2.2	2.3	2.4	2.5	2.6
0	16	1.15	1.2	1.3	1.4	1.5	1.6	1.7	1.8	1.9	2.0	2.1	2.2	2.3	2.4	2.5	2.6
100	17	1.15	1.2	1.3	1.4	1.5	1.6	1.7	1.8	1.9	2.0	2.1	2.2	2.3	2.4	2.5	2.6
100	18	1.15	1.2	1.3	1.4	1.5	1.6	1.7	1.8	1.9	2.0	2.1	2.2	2.3	2.4	2.5	2.6
100	19	1.15	1.2	1.3	1.4	1.5	1.6	1.7	1.8	1.9	2.0	2.1	2.2	2.3	2.4	2.5	2.6
100	20	1.15	1.2	1.3	1.4	1.5	1.6	1.7	1.8	1.9	2.0	2.1	2.2	2.3	2.4	2.5	2.6
100	21	1.15	1.2	1.3	1.4	1.5	1.6	1.7	1.8	1.9	2.0	2.1	2.2	2.3	2.4	2.5	2.6
100	22	1.15	1.2	1.3	1.4	1.5	1.6	1.7	1.8	1.9	2.0	2.1	2.2	2.3	2.4	2.5	2.6
100	23	1.15	1.2	1.3	1.4	1.5	1.6	1.7	1.8	1.9	2.0	2.1	2.2	2.3	2.4	2.5	2.6
100	24	1.15	1.2	1.3	1.4	1.5	1.6	1.7	1.8	1.9	2.0	2.1	2.2	2.3	2.4	2.5	2.6
100	25	1.15	1.2	1.3	1.4	1.5	1.6	1.7	1.8	1.9	2.0	2.1	2.2	2.3	2.4	2.5	2.6
100	26	1.15	1.2	1.3	1.4	1.5	1.6	1.7	1.8	1.9	2.0	2.1	2.2	2.3	2.4	2.5	2.6
100	27	1.15	1.2	1.3	1.4	1.5	1.6	1.7	1.8	1.9	2.0	2.1	2.2	2.3	2.4	2.5	2.6
100	28	1.15	1.2	1.3	1.4	1.5	1.6	1.7	1.8	1.9	2.0	2.1	2.2	2.3	2.4	2.5	2.6
100	29	1.15	1.2	1.3	1.4	1.5	1.6	1.7	1.8	1.9	2.0	2.1	2.2	2.3	2.4	2.5	2.6
100	30	1.15	1.2	1.3	1.4	1.5	1.6	1.7	1.8	1.9	2.0	2.1	2.2	2.3	2.4	2.5	2.6
200	31	1.15	1.2	1.3	1.4	1.5	1.6	1.7	1.8	1.9	2.0	2.1	2.2	2.3	2.4	2.5	2.6
200	32	1.15	1.2	1.3	1.4	1.5	1.6	1.7	1.8	1.9	2.0	2.1	2.2	2.3	2.4	2.5	2.6
200	33	1.15	1.2	1.3	1.4	1.5	1.6	1.7	1.8	1.9	2.0	2.1	2.2	2.3	2.4	2.5	2.6
200	34	1.15	1.2	1.3	1.4	1.5	1.6	1.7	1.8	1.9	2.0	2.1	2.2	2.3	2.4	2.5	2.6
200	35	1.15	1.2	1.3	1.4	1.5	1.6	1.7	1.8	1.9	2.0	2.1	2.2	2.3	2.4	2.5	2.6
200	36	1.15	1.2	1.3	1.4	1.5	1.6	1.7	1.8	1.9	2.0	2.1	2.2	2.3	2.4	2.5	2.6
200	37	1.15	1.2	1.3	1.4	1.5	1.6	1.7	1.8	1.9	2.0	2.1	2.2	2.3	2.4	2.5	2.6
200	38	1.15	1.2	1.3	1.4	1.5	1.6	1.7	1.8	1.9	2.0	2.1	2.2	2.3	2.4	2.5	2.6
200	39	1.15	1.2	1.3	1.4	1.5	1.6	1.7	1.8	1.9	2.0	2.1	2.2	2.3	2.4	2.5	2.6
200	40	1.15	1.2	1.3	1.4	1.5	1.6	1.7	1.8	1.9	2.0	2.1	2.2	2.3	2.4	2.5	2.6
200	41	1.15	1.2	1.3	1.4	1.5	1.6	1.7	1.8	1.9	2.0	2.1	2.2	2.3	2.4	2.5	2.6
200	42	1.15	1.2	1.3	1.4	1.5	1.6	1.7	1.8	1.9	2.0	2.1	2.2	2.3	2.4	2.5	2.6
200	43	1.15	1.2	1.3	1.4	1.5	1.6	1.7	1.8	1.9	2.0	2.1	2.2	2.3	2.4	2.5	2.6
300	44	1.15	1.2	1.3	1.4	1.5	1.6	1.7	1.8	1.9	2.0	2.1	2.2	2.3	2.4	2.5	2.6
300	45	1.15	1.2	1.3	1.4	1.5	1.6	1.7	1.8	1.9	2.0	2.1	2.2	2.3	2.4	2.5	2.6
300	46	1.15	1.2	1.3	1.4	1.5	1.6	1.7	1.8	1.9	2.0	2.1	2.2	2.3	2.4	2.5	2.6
300	47	1.15	1.2	1.3	1.4	1.5	1.6	1.7	1.8	1.9	2.0	2.1	2.2	2.3	2.4	2.5	2.6
300	48	1.15	1.2	1.3	1.4	1.5	1.6	1.7	1.8	1.9	2.0	2.1	2.2	2.3	2.4	2.5	2.6
300	49	1.15	1.2	1.3	1.4	1.5	1.6	1.7	1.8	1.9	2.0	2.1	2.2	2.3	2.4	2.5	2.6
300	50	1.15	1.2	1.3	1.4	1.5	1.6	1.7	1.8	1.9	2.0	2.1	2.2	2.3	2.4	2.5	2.6

FIGURE B.2. SAMPLE PRINTOUT FOR S2D CODE



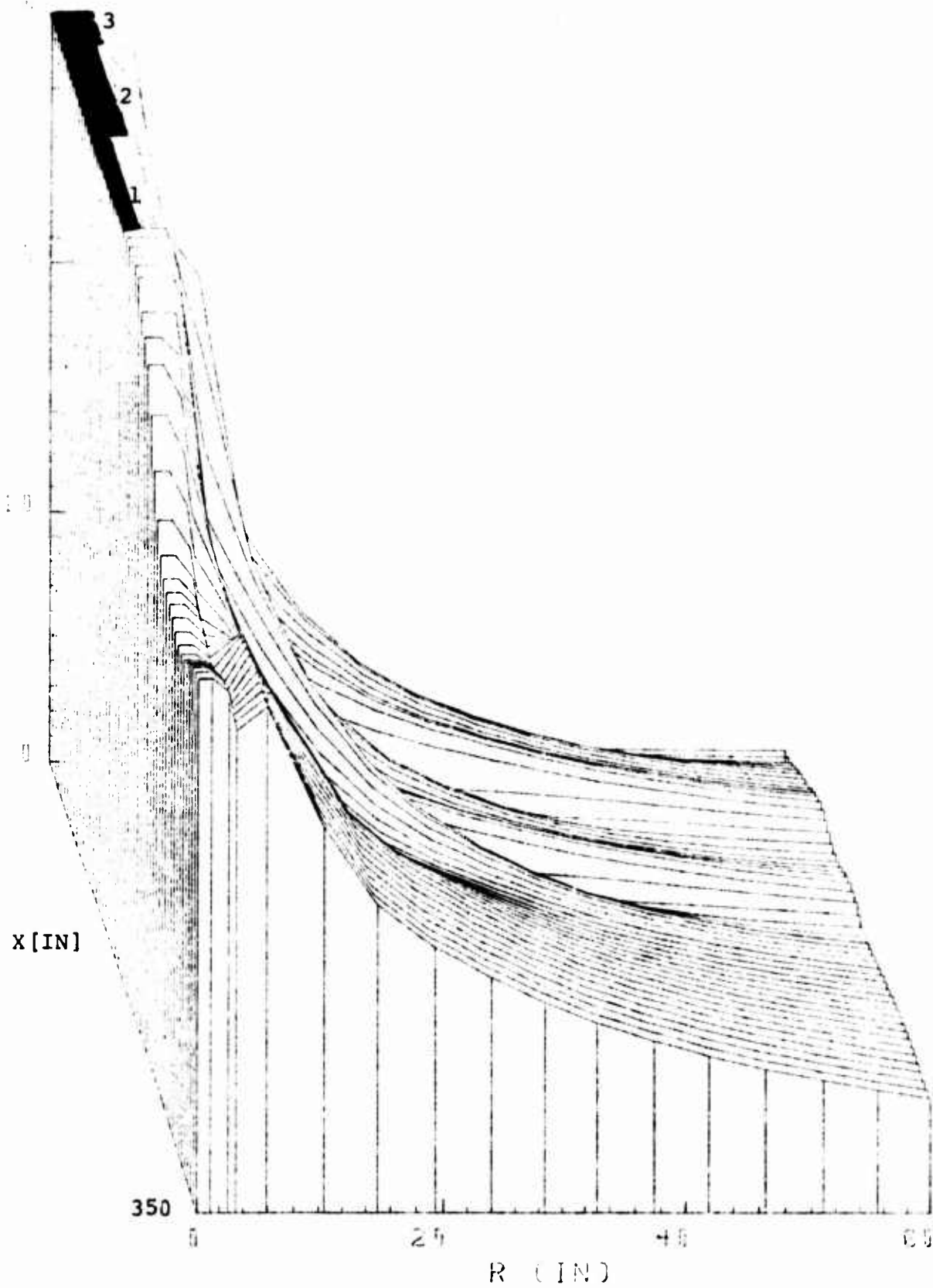


Figure B.3. Three-Dimensional Plot of External Peak Overpressure Field

APPENDIX C

THERMODYNAMIC CONSIDERATIONS

The following thermodynamic considerations were involved in the development and operation of the computer codes discussed in the text.

C.1 Chamber Thermodynamics

Estimates of chamber density and temperature for blast field calculations were made for various pressure profiles by several methods. Chamber temperature was estimated by one of the following three methods:

- 1) Chamber temperature constant and equal to flame temperature at maximum chamber pressure
- 2) Chamber temperature constant and equal to 0.9 of flame temperature at maximum chamber pressure
- 3) Chamber temperature varying adiabatically from the flame temperature at maximum chamber pressure

These different methods led to calculated free field peak pressure differences on the order of 10%. Method 2) was concluded to be the most realistic and was used for all final comparisons of calculated and experimental data.

Chamber densities were calculated from the pressures and temperatures from the general gas law

$$p = z\rho RT$$

where z was assumed constant and was determined from results of theoretical calculations for conditions representative of maximum chamber pressure and temperature (Ref. 4).

C.2 Nozzle Internal Thermodynamics

The fluid dynamic process from the combustion chamber to the exit of the nozzle was assumed to be adiabatic with a polytropic exponent equal to the ratio of specific heats of $\gamma = 1.22$. This assumption appeared fairly realistic for the range of temperatures, pressures and velocities and gas composition involved.

C.3 External Field Thermodynamics

The two-dimensional S2D computer code utilized in this report required the use of a single value of specific heat ratio γ to characterize the fluid flow process external to the nozzle. Since in actuality γ could vary from a minimum of about 1.2 in the hot combustion products directly at the nozzle exit to a maximum of 1.4 in the surrounding low temperature air, some compromise was necessary. In our calculations we used values of either $\gamma = 1.2$ or $\gamma = 1.4$. The latter value gave field pressures in regions of interest on the order of 30 percent larger and gave better agreement with experimental pressures. It was our conclusion that the larger value of γ is more appropriate to evaluation of the peak field pressures (which occur in the air where $\gamma = 1.4$) and this value was used for all data correlation comparisons.